Russian Geology and Geophysics © 2020, V.S. Sobolev IGM, Siberian Branch of the RAS
Vol. 61, No. 5–6, pp. 611–633, 2020 DOI:10.15372/RGG2019185
Geologiya i Geofizika

Petrology, Geochemistry, and the Origin of Sulfide-Bearing and PGE-mineralized Troctolites from the Konnikov Zone in the Yoko-Dovyren Layered Intrusion

A.A. Ariskin[a,b,] ✉, L.V. Danyushevsky[c], M. Fiorentini[d], G.S. Nikolaev[b], E.V. Kislov[e], I.V. Pshenitsyn[a,b], V.O. Yapaskurt[a], S.N. Sobolev[a]

[a] *Lomonosov Moscow State University, Leninskie Gory 1, Moscow, 119234, Russia*

[b] *Vernadsky Institute of Geochemistry and Analytical Chemistry, Russian Academy of Sciences, ul. Kosygina 19, Moscow, 119991, Russia*

[c] *CODES CoE and Earth Sciences, University of Tasmania, Private Bag 79, Hobart, TAS 7001, Australia*

[d] *Centre for Exploration Targeting, School of Earth Sciences, ARC Centre of Excellence for Core to Crust Fluid Systems,*
The University of Western Australia, 35 Stirling Highway, 6009 Crawley, Perth, Western Australia, Australia

[e] *Geological Institute, Siberian Branch of the Russian Academy of Sciences, ul. Sakh'yanovoi 6, Ulan-Ude, 670047, Russia*

Received 21 March 2019; accepted 10 October 2019

Abstract—The exposures, structure, mineralogy, and composition of unusual sulfide-bearing troctolites from the Yoko-Dovyren layered intrusion in the northern Baikal area (Russia) are described in detail for the first time. The troctolite succession (referred to as the Konnikov Zone) is characterized by the presence of pegmatoid poikilite sulfides and sulfide dissemination with diverse PGE mineralization. The former are dominated by pyrrhotite–troilite products of exsolution of monosulfide solid solution (mss), and the latter is composed mostly of cubanite–chalcopyrite assemblages produced from an intermediate Ni–Cu–Fe solid solution (iss). The positive covariations between the contents of sulfur and chalcogens (Se, Te) along with the sublinear dependence of the Pd, Pt, Au, and Cu contents on the Te contents indicate a sulfide control of the distribution of these elements in troctolite cumulates. According to the sulfide-normalized contents of these elements in rocks, the average "100% sulfides" in the samples are subdivided into two groups: (1) strongly depleted in PGE, Au, Cu, and Te and (2) with 10–50-fold enrichment in them. This division is consistent with the morphological and mineralogical differences between the groups. Of genetic significance is the fact that the mss assemblages are somewhat poorer in PGE and Te than the primitive sulfides from the Dovyren basal zone, whereas the assemblages with predominant copper sulfides are significantly richer in these elements. This fact is confirmed by LA-ICP-MS data on the trace-element composition of the sulfide phases. The established specific features indicate a limited scale of fractionation of immiscible sulfides during the solidification of the troctolite cumulates. The formation of PGE- and Te-rich assemblages can be related to the course of crystallization of a sulfide precursor similar to the most primitive sulfide liquid. This is consistent with the known laws of crystallization of sulfide systems and explains the abnormally high S/Te ratios in pegmatoid troctolites enriched in mss products. Thus, sulfide melts act as an agent that transports precious metals and chalcogens in the troctolite cumulate area. This conclusion requires specification of the physical mechanisms and parameters (rheology, permeability, wettability by sulfides of different phases, etc.) of the cumulus medium favoring the spatial separation of a monosulfide solution and Cu-containing PGE-rich fractions with their subsequent infiltration and deposition at the boundaries of critical low permeability.

Keywords: sulfide-bearing troctolite, mss, iss, PGE mineralization, precious metals, fractionation of Se *and* Te, *sulfide separation, infiltration, accumulation, Dovyren*

INTRODUCTION

The Yoko-Dovyren intrusion is located 60 km northeast of the tip of Lake Baikal (Northern Baikal, Russia), lies among the carbonate-terrigenous (mainly black-shale) strata of the Synnyr Rift (Konnikov, 1986; Rytsk et al., 2002), and belongs the Synnyr–Dovyren volcano-plutonic complex with an age of 724–728 Ma (Ariskin et al., 2013; Ernst et al., 2016). In addition to the main layered massif with a length of ~26 km, it comprises underlying gabbro-peridotite sills and dikes of leucocratic gabbronorite (Kislov, 1998; Ariskin et al., 2018b; Orsoev et al., 2018). These intrusive and subvolcanic bodies are overlapped by the effusive formations of the Synnyr Rift, including high-Ti basalts of the Inyaptuk Formation and low-Ti basaltic andesites of the Synnyr Formation (Manuylova and Zarubin, 1981). Isotope-geochemical data indicate a genetic relationship between the intrusive rocks and volcanics of the low-Ti series (Ariskin et al., 2015a).

✉ Corresponding author.
E-mail address: ariskin@rambler.ru (A.A. Ariskin)

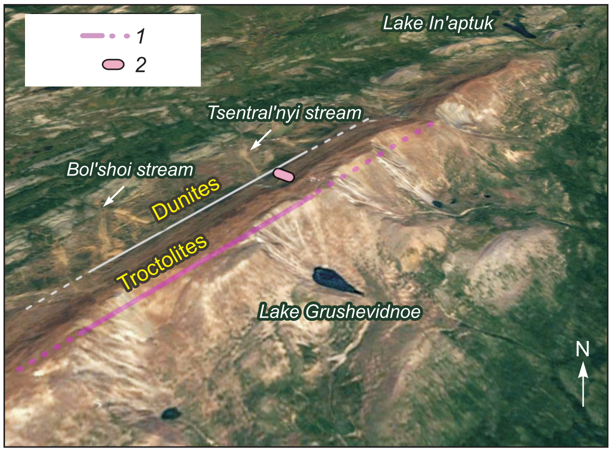

Fig. 1. Middle and northeastern part of the Dovyren Mountain with the location of the exposures of sulfide-bearing and PGE-mineralized troctolites. *1*, Main Reef, *2*, investigated interval.

The dipping of Dovyren is close to vertical, which allows one to reconstruct its stratigraphic cross sections in the primary subhorizontal occurrence by means of testing surface exposures across the strike of the intrusion. The structure of this pluton has been studied in detail in its thickest central part (3.2–3.4 km), in the vicinity of the Bol'shoi and Tsentral'nyi streams (Kislov, 1998; Ariskin et al., 2018b) (Fig. 1). At the base of the cross section, there are endocontact rocks (chilled gabbronorites and picrodolerites and plagioclase lherzolites above), followed by the main stratigraphic succession including five zones corresponding to changes in cumulus assemblages (from bottom to top): dunite (Ol + Chr) → troctolite (Ol + Pl + Chr) → olivine gabbro (Pl + Ol + Cpx ± Opx) → olivine gabbronorite (Pl + Ol + Cpx ± Opx) → quartz gabbronorite and pigeonite-containing gabbro (Pl + Cpx ± Opx ± Pig)[1] (on the left of Fig. 2). Gabbro-pegmatites and quartz granophyres are widespread in the uppermost part of the intrusion. The upper contact zone is composed of fine-grained gabbronorites.

The interest in the problems of the origin of sulfides and the ore potential of the Dovyren Intrusive Complex is due to the occurrence of Cu–Ni sulfide ores in the underlying sills and in the basal part of the pluton (Gurulev, 1965; Konnikov, 1986), as well as the presence of feldspar-rich rocks (up to anorthosites) hosting low-sulfide mineralization rich in platinum group elements (PGEs) – the so-called Main Reef or Reef I (Distler and Stepin, 1992; Orsoev et al., 1995; Kislov, 1998; Konnikov et al., 2000) (Fig. 2). For many years, the attention of experts has been focused on studying the composition of rocks and PGE mineralization of the Main Reef, which actually represents a 150-m thick horizon adjacent to a nominal boundary between troctolites and olivine gabbros. Such a transitional stratigraphic contact is manifested in the form of irregular intercalation of melanocratic to leucotroctolites and olivine gabbros with numerous schlieren and anorthosite interlayers, which are often associated with gabbropegmatites. The PGE enrichment in some of the anorthosite schlieren is the reason for calling this zone Critical – by analogy with the known horizons in the Bushveld intrusion (Tolstykh et al., 2008; Orsoev, 2019). However, the analogies end here, and neither pyroxenites nor thin chromite interlayers as important components of the Bushveld rocks are observed in the Dovyren sections. It is more important that the structural position of pyroxene phases in all types of the transition rocks indicates their intercumulus nature, which allows one to consider the observed association as olivine-plagioclase cumulates with varying proportions of olivine, plagioclase, and crystallization products of intercumulus melt (Ariskin et al., 2018b).

The field works at the Dovyren intrusion resulted in establishing a low-sulfide (noble-metal at certain sites) mineralization in the lower half of the troctolite zone, located in a stratigraphic range from about 40 to 480 m above the "washed" contact with dunites (Ariskin et al., 2015b). The rocks of this part of the cross section (called the Konnikov Zone, see below) noticeably differ from the platinum-bearing anorthosites and leucogabbro of the Main Reef not only in terms of their bulk composition, but also in the morphology of sulfide occurences, the presence of pegmatoid sulfides, trace-element composition of the sulfide phases, and the composition of PGE minerals (PGMs). This is the reason for separating sulfide-bearing troctolites into a specific genetic type of low-sulfide mineralization, which seems to represent an important part of the sulfide history in the Dovyren chamber, related to the transfer and concentration of noble metals in the strata of crystallizing troctolite cumulates (Ariskin et al., 2018b).

The first discovery of sulfide-bearing troctolites took place in 2007 in the waterheads of the Tsentral'nyi stream, about 100 m above the stratigraphic contact between dunites and the troctolite zone (Fig. 1). A large block of troctolite with nests of sulfide mineralization was discovered here among the rock debris by Jonus Motta-e-Silva (Brazil) and E.V. Kislov (Russia). One of the samples (07DV403-1) contained a spheroid inclusion of about three cm in size, represented by an olivine-plagioclase matrix with fragmented impregnations of sulfides in the interstices between the grains of rock-forming minerals. On the polished sections of the sample, the inclusion was clearly rounded, with a submillimeter halo of rarer disseminated sulfides. In 2010, during LA-ICP-MS studies of the tracke element compositions of sulfide phases in the Dovyren rocks, E.G. Konnikov and colleagues found high concentrations of Pd in pentlandite (91 ± 84 ppm, $n = 7$) from this sample, at a maximum of up to 250 ppm[2]. These values are close to the average Pd content in pentlandite from the PGE anorthosites of the Main Reef of Dovyren (235 ± 84 g/t, $n = 10$) (Ariskin et al., 2015b).

Successive studies of the 07DV403-1 sample using the scanning electron microscopy (SEM) methods at the Uni-

---

[1] Here and below: Pl, plagioclase, Ol, olivine, Cpx, clinopyroxene, Tr, troilite, Po, pyrrhotite, Pn, pentlandite, Cub, cubanite, Cpy, chalcopyrite, Alt, altaite, Tln, talnachite, Chr, alumochromite, Pig, pigeonite.

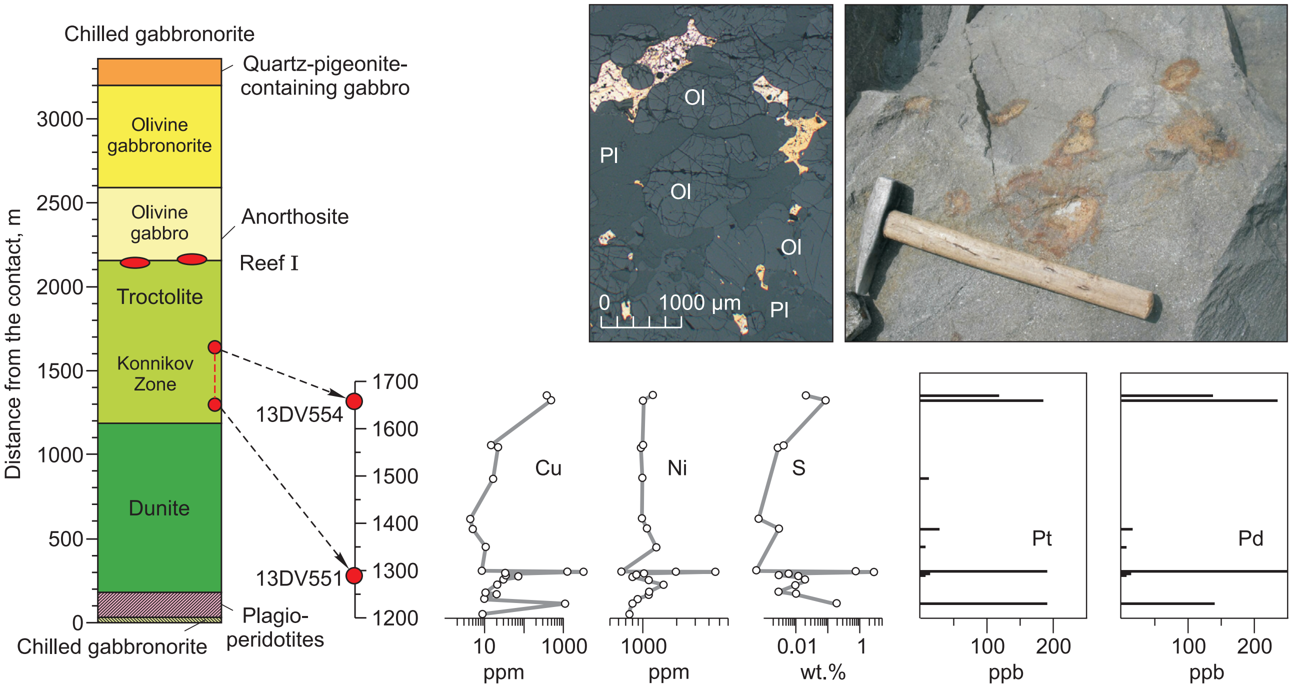

Fig. 2. Structure of the Yoko-Dovyren intrusion (Ariskin et al., 2018b) and the Cu, Ni, S, Pt, and Pd distribution in the lower half of the troctolite zone. The inset to the left shows the microphotograph of the thin section of the 07DV403-1 sample (the yellow phase is chalcopyrite) and the photograph of the outcrop of troctolites with sulfide impregnation schlieren from approximately the same stratigraphic level (right). The Konnikov Zone has a thickness of about 400 m (see the dashed arrows). The red circles indicate the samples studied in detail from the 13DV551 (near site 07DV403-1) and 13DV554 sampling points.

versity of Tasmania (Hobart, Australia) allowed identifying 12 grains of moncheite $Pt(Te,Bi)_2$ and michenerite PdBiTe from 1 to 9 μm in size. The Bi and Te proportions were approximately equal, and one grain corresponded to the rhodium moncheite with a content of 6 wt.% Rh. In addition, two grains of Ag–Au phases with a size of 1 and 8 μm were found. All of them were confined to sulfide interstices between the grains of cumulus olivine and poikilitic plagioclase. In the least altered rock fragments not affected by secondary changes, the orthomagmatic relations of olivine, plagioclase, and sulfides were observed (see the thin section in the inset in Fig. 2), represented by the assemblage of pyrrhotite, pentlandite, chalcopyrite, and cubanite as the products of crystallization of copper-rich sulfide solutions. These observations indicated a certain analogy with the PGE mineralization of the Main Reef (Orsoev et al., 1995; Tolstykh et al., 2008), especially as the average mineral composition of sulfides in troctolites (over 70% of cubanite and chalcopyrite estimated by means of a Mineral liberation analysis (MLA)) turned out to be close to that from platinum-bearing anorthosites (Ariskin et al., 2018b).

As a result, the task is to search for original exposures of sulfide-bearing rocks in the lower part of the troctolite zone and collect representative samples for the next study. This article summarizes data on samples from the Konnikov Zone, including both mineralogical and geochemical characteristics of the rocks, the composition of sulfides, and the diversity of PGMs. In the final section, the possible genetic links between PGE-poor and PGE-rich sulfide assemblages are considered.

Analytical studies come down to examining the composition of rock-forming minerals, sulfide phases, and platinum group minerals, as well as determining the whole-rock composition of the rocks.

Microprobe analysis was carried out at the Central Science Laboratory of the University of Tasmania (Hobart, Australia) and the Laboratory of local methods of material studies at the Department of Petrology of the Faculty of Geology (Lomonosov Moscow State University, Russia). The former was performed using a Cameca SX-100 EPMA electron microprobe with five wave spectrometers and a Bruker energy dispersive attachment, and the latter using a JSM-6480LV electron microscope with a tungsten thermionic cathode equipped with an X-Max-N50 energy dispersive spectrometer (Oxford Instruments, UK). Standards and samples were measured in a focused probe mode: at an accelerating voltage of 15 kV, a current strength of 20 ηA on the probe and a beam size of 5 μm (15 kV, 30 ηA, and 2 μm for olivine and spinel) in Tasmania, and all minerals at 20 kV and 10 ηA at Moscow State University. The international standards USNM 115900 (LPL plagioclase), USNM 122142 (KANZ augite), APAT, HORN, USNM 111312/444 (San Carlos olivine), and USNM 117075 (chromite from New Caledonia) were used as the standards in Tasmania

(Jarosewich et al., 1980). When working at the Department of Petrology at Moscow State University, the standards of pure metals, stoichiometric oxides, and sulfides were used. The accuracy of measuring the contents of the major elements varied in a range of 0.5–2.0 rel.%.

At the initial stage of determination the PGMs and Ag-Au minerals in UTAS (2010–2014), a Hitachi SU-70 FESEM ultra-high resolution field electron microscope was used, which allowed to visualize the surface details of a nanometer-sized sample. The first PGM compositions (including detailed zoning of largest grains) were obtained using this device, equipped with an X-Max 80 energy dispersive spectrometer.

The concentrations of Fe, Ni, Cu, Co, Se, Te, Zn, Mo, Ag, Cd, Sb, Pb, Rh, Os, Ir, Ru, Rh, Pt, Pd, Re, and Au in sulfides were determined by means of laser ablation inductively coupled plasma mass spectrometry (LA-ICP-MS) at the School of Physical Sciences and the Centre for Ore Deposit and Earth Sciences at the University of Tasmania (CODES, Hobart, Australia). Analytical equipment comprises two laser ablation microprobes: YAG instrument from New Wave Research and a RESOlution S-155 (using a 193-ηm excimer laser from Resonetics), both coupled with an Agilent 7700s quadrupole mass spectrometer. The laser beam size is 22–40 μm at a pulse frequency of 5 Hz in pure helium atmosphere. The details of standards and corrections for the interference of individual elements and software are presented in (Ariskin et al., 2016, 2018b).

The whole-rock compositions (including PGEs) were studied at the GEOLABS laboratory in Sudbury (Ontario, Canada), see (www.mndm.gov.on.ca/sites/default/files/2017_ geo_labs_brochure.pdf). The concentrations of the major elements (as well as Cu, Ni, and Co) were obtained according to a standard XRF analysis. Gold, silver, selenium, and tellurium were determined by an ultra-trace ICP-MS method following an aqua regia digestion procedure with the detection limits varying as follows: Au = 0.4 ppb, Ag = 2–10 ppb, Se = 0.04–0.1 ppm, and Te = 0.01–0.02 ppm. The concentrations of Ir, Ru, Rh, Pt, and Pd are determined via ICP-MS following fire fusion, with the these detection limits: 0.01 for Ir, 0.08 for Ru, 0.04 for Rh, 0.12 for Pd, and 0.17 ppb for Pt.

Estimates of the relative proportions of sulfide phases in the samples (Pn/Po/Cpy/Cub) are obtained by automated identification of minerals on a FEI Quanta 600 scanning electron microscope equipped with an EDAX Sapphire SUTW Si (Li) energy dispersive spectrometer using the MLA (Mineral Liberation Analyzer) software package. In this case, two methods are used – XMOD_STD and SPL_Lt, which provide a “frame” resolution for scanning local areas of the order of 12 μm^2 and ~3 μm^2 in size, respectively (Ariskin et al., 2016). The measurements are carried out on polished mounts with a diameter of 1 inch. In the case of XMOD_STD, this size yields about 10,000 spectra of minerals, which made it possible to reliably estimate the “average sulfide composition” even for poor mineralization with sulfur contents of <0.1 wt.% The relative proportions of Pn, Po, Cpy, and Cub are calculated by normalizing the corresponding areas or the number of “hits” for a particular sulfide mineral.

PETROGRAPHY AND MINERALOGY OF SULFIDE-BEARING TROCTOLITES

Selection of samples. In the field season of 2013, a search was made for original exposures and new samples of mineralized troctolites in the waterheads of the Tsentral’nyi stream across the strike of the intrusion: within a ~200-m wide strip, parallel to the edges of both slopes of the stream (Fig. 1). At the stratigraphic level, slightly higher than the site at which the sample 07DV403-1 was discovered, the original exposures of troctolites with scattered sulfide nests were discovered (Fig. 2, inset to the right). Not far from the

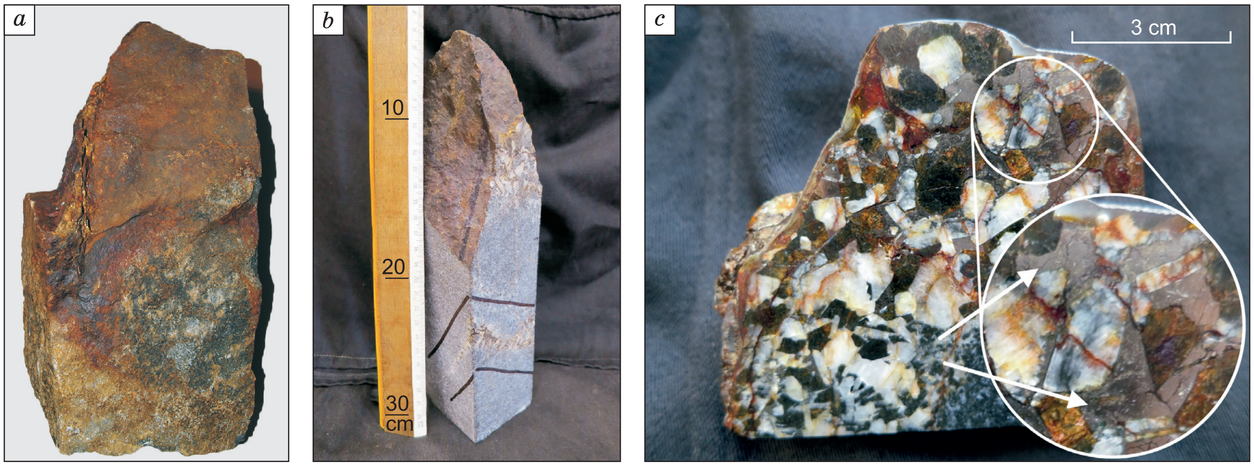

Fig. 3. Original sample of the 13DV551-4a mineralized troctolite (*a*), the product of its sawing with a vein and a sulfide-bearing “blotch” *(b),* and the demonstration sample of pegmatoid troctolite with abundant sulfides *(c)*, cut from the top of the sample into parts *b*. The arrows in the part *c* indicate xenomorphic sulfides (gray).

first finding (sampling site 13DV551, Fig. 2), there was another block of troctolite up to 40 cm across, containing round sulfide nests with a diameter of 1 to 3 cm. Several rocks samples were selected (13DV551-1, -2, and -3), but the most interesting was a 10 × 15 × 50-cm angular block split into several fragments with pegmatoid sulfide veins whose thickness reached as large as 1 cm. Several fragments were collected, the largest of which (13DV551-4a) is shown in Fig. 3*a*. The pegmatoid grains of olivine and plagioclase with abnormally large xenomorphic sulfides in the intergranular space are clearly visible on the cuts of this sample (Fig. 3*b*) and the demonstration sections (Fig. 3*c*). This is the first discovery of sulfide-bearing pegmatoid troctolites in Dovyren.

Another original outcrop was discovered at the source of the Tsentral'nyi stream, among rocky exposures under a slope heading, at a distance of about 460 m above the contact between troctolites and dunites (site 13DV554, Fig. 2). Sample 13DV554-4 (Table 1) was collected directly from the outcrop and fragments of schlieren and segregations of heterogeneous material (Ol + Pl + sulfide) up to 5–10 cm in size were found among the rock debris at the base of these outcrops. One of these pieces (13DV554-1) contained a fragment of a relatively large schlieren with a diameter of ~5 cm, from which 12 polished sections were made. Two of them, representing opposite parts of this heterogeneous schlieren (samples 13DV554-1-3 and -12), were studied in detail, with the data on sulfide phases and PGE minerals available below. In the 2015 season, those materials were supplemented with samples with sulfide-poor mineralization, taken in the lower part of the Konnikov Zone (D8/15, D9/15, D10/15, D11/15, and D12/15) (Table 1).

Petrography. Like ordinary troctolites, their sulfide-bearing varieties are represented by massive medium-grained rocks of allotriomorphic-granular texture (Fig. 4*a,b*). The degree of idiomorphism and the average grain size are higher for olivine, which is superior to plagioclase (Table 1), and the amount of clinopyroxene does not exceed 1.5–2.0%. The only exception is D12/15 leucotroctolite in which the amount of plagioclase reaches 60% (Table 1). The dominance of olivine is not consistent with equilibrium proportions of crystallization on Ol-Pl cotectics (~ 70% of Pl and 30% of Ol), which emphasizes the primary cumulus nature of olivine and in situ crystallization of the main mass of plagioclase in the initial proto-olivine cumulate. The minor clinopyroxene (manifested in the form of rare interstices and the thinnest rims around olivine grains) indicates that the intercumulus melt almost completely "left" the cumulate precursor, apparently following the partial cotectic crystallization of plagioclase and olivine. This is consistent with the abnormally low contents of incompatible elements and sublinear trends in troctolite compositions in the ternary petrochemical diagrams, indicating a bimineral mixture of olivine and plagioclase crystals (Ariskin et al., 2018b, Fig. 15).

An increased amount of plagioclase correlates with fingerprints of foliation in individual thin sections (Fig. 4*b*), which can be considered as a result of deformation of origi-

Table 1. Stratigraphic position and specific features of the composition of sulfide-bearing and nonmineralized troctolites

No.	Sample	*h*, m*	Rock	CIPW, wt.%		Composition, mol.%		S, wt.%	Cu, ppm
				Ol	Pl	Fo (Ol)	An (Pl)		
1	07DV313-2	1208	Troctolite	56	43	85.8 ± 0.3	87.4 ± 0.7	<0.01	8.9
2	**D12/15**	1231	Sulfide-bearing leucotroctolite	37	60	83.3 ± 0.3	87.1 ± 0.4	0.19	1084
3	07DV314-2	1251	Troctolite	74	24	82.0 ± 0.2	86.9 ± 2.8	0.01	20.3
4	07DV314-4	1281	»	77	22	84.2 ± 0.1	87.0 ± 0.5	0.02	30.0
5	**07DV403-1**	1288	Troctolite**	55	44	84.6 ± 0.2	87.2 ± 2.1	0.01	72.5
6	**D9/15**	1291	»	75	24	83.2 ± 0.1	86,4 ± 0.5	0.003	34.0
7	**D8/15**	1294	»	67	31	82.1 ± 0.3	85.2 ± 0.9	0.006	33.0
8	**13DV551-4a**	1298	Pegmatoid troctolite	50	41	82.5 ± 0.2	84.7 ± 0.7	2.82	3335
9	**13DV551-4e**	1298.3	Sulfide-bearing troctolite	60	38	82.6 ± 0.4	85.6 ± 1.2	0.76	1240
10	07DV403-2	1300	Troctolite	53	47	84.3 ± 0.1	85.7 ± 0.3	0.01	641
11	**D10/15 and D11/15**	1388	Troctolite**	74	25	83.1 ± 0.1	86.1 ± 1.2	0.003	5.1
12	**13DV554-1**	1660	Sulfide-bearing troctolite	57	42	84.0 ± 0.4	87.9 ± 1.8	0.09	486
13	**13DV554-4**	1670	»	70	29	84.5 ± 0.3	87.3 ± 1.1	0.02	372

Note. All samples are taken in the thalweg and in parallel to the sides of the Tsentral'nyi stream, across the extension of the intrusion at a distance of about 460 m along the slope (Fig. 1). Here and Table 2 samples with poor and very poor mineralization from the Konnikov Zone are highlighted in bold. The proportions of olivine and plagioclase are calculated from the whole-rock compositions assuming 5 rel.% of oxidized iron. The average compositions of these minerals are calculated from EPMA analyses of 5 to 20 grains. The low concentrations of sulfur and copper contents in some of the samples are explained by the uneven distribution of sulfides and the preliminary selection of rare fragments with disseminated sulfides for LA-ICP-MS studies. In this case, an insignificant amount of sulfide material falls into the specimen for XRF analysis.

* Stratigraphic reconstruction of the distance from the lower contact of the Yoko-Dovyren intrusion with respect to the generalized cross section along the Bol'shoi stream according to (Ariskin et al., 2018b), with some clarifications added. In this case, the stratigraphic level of the nominal contact between dunites and troctolites is assumed to be 1190 m.

** Very poor sulfide mineralization is determined (see the image of the thin section for the 07DV403-1 sample in Fig. 2).

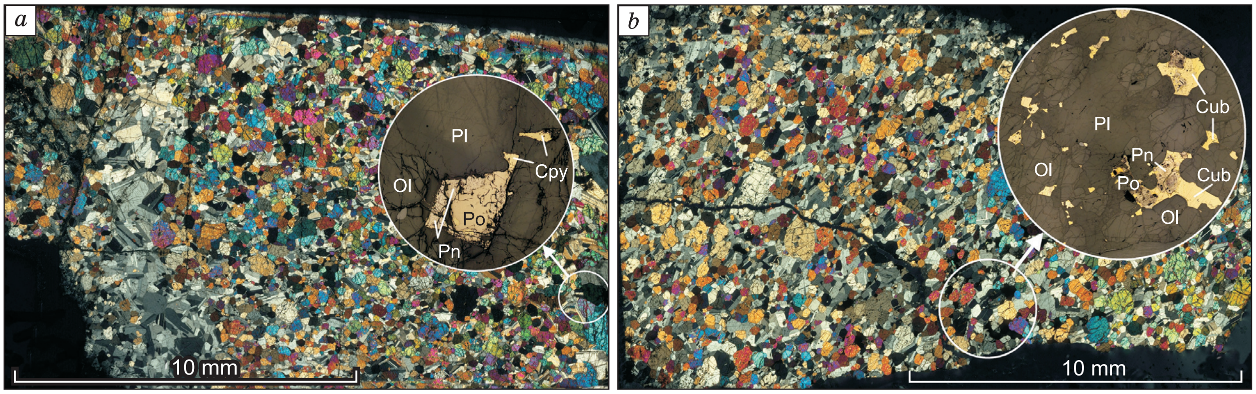

Fig. 4. High-resolution microphotographs of sulfide-bearing troctolites, obtained by scanning thin sections using polarizing films. *a,* The 13DV551-4a sample with veins of the feldspar-rich material and the contact with pegmatoid troctolite; *b*, the 13DV554-1 sample from which thin sections are cut for studying the sulfide phases and PGE minerals. In this sample, the orientation of mineral grains is traced, probably reflecting deformations during compaction and recrystallization of the initial cumulate (see the text).

nal cumulates (probably during their compaction), additional crystallization, and upward infiltration of the residual melt (Holness et al., 2017). During field and textural examinations, the confinement of sulfide mineralization to the more leucocratic sections of troctolites is seen, but this conclusion requires more detailed studies for further confirmation. An interesting fact is that rare pyroxene rims more often occur at the grain boundaries between cumulus olivine and sulfide phases.

The compositions of olivine and plagioclase in sulfide-bearing and non-mineralized troctolites vary within narrow limits — usually 83–85% of Fo and 86–88% of An (Table 1). Al-Cr spinel contains 10–13 wt.% of Al_2O_3 and 36–40 wt.% of Cr_2O_3, while the spinel mg# = $Mg/(Mg + Fe^{2+})$ varies around 0.24. This constancy of the composition of the minerals leaves little doubt that the observed differences in the amount of plagioclase in troctolites are due to different degrees of accumulation of cumulus olivine, which is in equilibrium with cotectic plagioclase and the melt.

Mineralogy of sulfide phases. Troctolites from the Konnikov Zone are characterized by two structural-morphological types of sulfide associations: 1) disseminated impregnation in sulfide-bearing schlieren, which is net-textured[2] at certain regions, and 2) pegmatoid occurrences of xenomorphic grains. Using the MLA method for estimating the average mineral composition in the samples, it is shown that assemblages with the predominance of copper-rich minerals prevail in the first case and that the Fe-Ni phases with (Po ± Tr): Pn~2:1 predominate in the second one (Table 2). In all the cases, cubanite is superior to chalcopyrite. One sample from the lower part of the Konnikov Zone (13DV551-2-2) has intermediate characteristics. Structural studies including a microprobe analysis suggest that the disseminated sulfides are mostly represented by the crystallization products of copper-rich sulfide liquids whose composition is probably close to that of Ni-Cu-Fe high-temperature cubic sulfide solid solutions iss_1 and iss_2[3]. Both are noted for lamellar exsolution structures formed by troilite and Fe-pyrrhotite as a result of the low-temperature transformation of a high-*T* solid pyrrhotite solution (Fig. 5*a,b*).

In pyrrhotite and cubanite, thin lamellae of pentlandite exsolution are not uncommon. The late generations of cubic sulfide solutions (iss_3 and iss_4, which are richer in Cu and poorer in Fe) are less common. These associations are characterized by accumulations of small lamellae and segregations of pentlandite, which tend to associate with chalcopyrite in troilite and pyrrhotite intergrowths (Fig. 5*c*). There are very rarely encountered grains corresponding to a late low-temperature solution of iss_5, whose structural feature is the lattice intergrowths of chalcopyrite with talnahite $Cu_9Fe_8S_{16}$ and large pentlandite segregations (Fig. 5*d*). In chalcopyrite crystals, twins of the cubic → tetragonal polymorphic transition are often observed. This association contains small sphalerite grains and the smallest (often isometric) inclusions of galena rarely exceeding 5 µm in size. Net-textured

---

[2] The term “net-textured” is applied to localized areas of thin sections and rock mounts with a maximum content of disseminated sulfides, whose distribution suggests local connectivity of the sulfide matter on a scale of several millimeters (Fig. 4*b*).

[3] The description of solid sulfide solutions is given in a genetic sequence (from early to late ones), established by the study of ore samples from the Norilsk region and confirmed by observations for the sulfide-bearing Dovyren rocks (Spiridonov, 2010; Spiridonov et al., 2019a,b): mss_1 (as intergrowths of troilite, Fe-pyrrhotite, and pentlandite) → mss_2 (Tr + Pn + Po with minor Cpy) → iss1 (Tr + Cub with inclusions of Pn) → iss2 (lattice intergrowths of Cpy + Cub with inclusions of ferrous Po and Pn) → iss3 with typical exsolution structures of cubanite (matrix) – chalcopyrite (lamellae) → iss4 (two-stage exsolution structures – cubanite in the chalcopyrite matrix) → iss5 (lamellar intergrowths of chalcopyrite and talnakhite plus pentlandite with no cubanite), see notes for the microphotographs in Fig. 5. The unambiguous identification of the origian exsolution structures of mss and iss is complicated by annealing of sulfides during the long history of solidification of the Yoko-Dovyren intrusion (Ariskin et al., 2018b), which results in that most sulfide grains have been recrystallized to form granular intergrowths of troilite, pyrrhotite, cubanite, pentlandite, and chalcopyrite (Fig. 6).

Table 2. Proportions of sulfide phases in the mineralized troctolites (according to the MLA results)

Sample	Type of impregnations	Method	Mineral phases, %*			
			Po ± Tr	Pn	Cpy	Cub
Sulfides in picrodolerite from the chilled zone						
DV30-1	Rare nests	XMOD_STD	78.6	12.0	8.7	0.7
Sulfides in the rocks of the lower part of the Konnikov Zone						
07DV403-1	Schieren with disseminated impregnations	XMOD_STD	5.0	15.1	10.1	69.8
07DV403-1a***		»	15.4	9.6	8.7	66.4
13DV551-2-2	The same	»	20.7	23.3	4.5	51.6
		SPL_Lt	22.5	37.7	9.6	30.2
13DV551-4b-4	Pegmatoid	»	49.8	26.7	4.0	19.5
Sulfides in the rocks of the upper part of the Konnikov Zone						
13DV554-1-3	Schieren with disseminated impregnations	XMOD_STD	10.9	14.0	20.5	54.7
		SPL_Lt	9.6	16.7	15.5	58.2
13DV554-1-12	The same	XMOD_STD	10.9	12.2	3.0	73.9
		SPL_Lt	8.5	19.8	9.3	62.5

Note. For comparison, the composition of primitive sulfides from the chilled zone of the Yoko-Dovyren intrusion is given (Ariskin et al., 2018c). The differences between the XMOD_STD and SPL_Lt methods are given in the text. The "Cub" denotation refers to the stoichiometric phase of the corresponding composition and, in some cases, to a highly cuprous phase with variable Cu:Fe. The 13DV551-2-2 sample is taken from the debris near the sample with pegmatoid sulfides (13DV551-4, see Table 1).

* The proportions of sulfide minerals are estimated as the ratio of the area of the tested microplates to the total area of sulfides in the sample.

*** In the case of the 07DV403-1 sample, the data for two mounts are given.

sulfides may occasionally contain rare small crystals of a high-T hexagonal Ni-Fe solid solution, possibly mss$_1$.

Pegmatoid veins of troctolites in the lower parts of the Konnikov Zone are characterized by large xenomorphic sulfides similar to olivine and plagioclase crystals, thereby reaching 5–6 mm in size. Sulfide phases fill the space between the grains of silicate minerals, forming a poikilitic-like matrix. Their phase composition noticeably differs from schieren enriched in cuprous sulfides (Fig. 5; Table 2). This is manifested in the sharp predominance of pyrrhotite that associates with pentlandite and cubanite, with troilite occurring only occasionally. As compared to other mineralized troctolites, the sulfides are much more altered here as mackinavite (Fe, Ni)$_9$S$_8$ (tetragonal) and violarite (FeNi$_2$S$_4$) are often found, including minor pyrite. "Fresh" pyrrhotite and pentlandite are rarely observed. All these sulfide phases are encountered in close association and relatively evenly distributed over the sulfide nests and pegmatoid veins (Fig. 6*a,b*). The size of individual grains of pyrrhotite may reach several millimeters. Although typical snake-like structures of the exsolution of mss into a mixture of pyrrhotite and troilite are not observed here, this association is regarded as the exsolution product of a high-temperature hexagonal nickel-ferrous solution. The search for relict primary structures for a more accurate specification of mss$_1$ or mss$_2$ is difficult, and it is partly due to the large size of the sulfide grains in individual polished sections, but to a greater extent, because of their complete recrystallization during prolonged annealing.

Platinum-group element minerals (PGMs) in troctolites are represented by mineral assemblages characteristic for low-sulfide mineralization from other ore-bearing intrusions (Godel et al., 2007; Oberthür, 2011; O'Driscoll and González-Jiménez, 2016). Pt and Pd tellurides and bismuthotellurides predominate, while their stannides and plumbides along with altaite PbTe and associated Au–Ag minerals are less common. Among Pd (± Pt) stannides, paolovite Pd$_2$Sn is found more often, but atokite Pd$_3$Sn is rare. In addition, the presence of an unidentified stannide with a ratio of Pd : Pt ~ 2 is established. Among other relatively common palladium minerals, zvyagintsevite Pd$_3$Pb and polarite PdHg is found in the upper part of the Konnikov Zone (Fig. 7d). The "mercury specialization" of this part of the section corresponds to the presence of Hg-containing PGMs in anorthosites from the Main Reef (Table 3), with this being a unique feature of the platinum metal mineralization of the Yoko-Dovyren pluton (Spiridonov et al., 2019a,b). Sperrylite PtAs$_2$ is extremely rare, with only a few grains with a size of <5 µm found in troctolites. The low occurrence of sperrylite is also a characteristic feature of PGE-mineralized and ore-bearing rocks of Dovyren (Tolstykh et al., 2008). Rock areas subjected to secondary alterations are noted for the presence of low-temperature, possibly late metasomatic grains of silver minerals, which often occurs in the form of low-standard electrum, native silver, argentite Ag$_2$S, and hessite Ag$_2$Te. They compose growths and microveins in sulfides and in a silicate matrix with a size of no more than 3–5 µm.

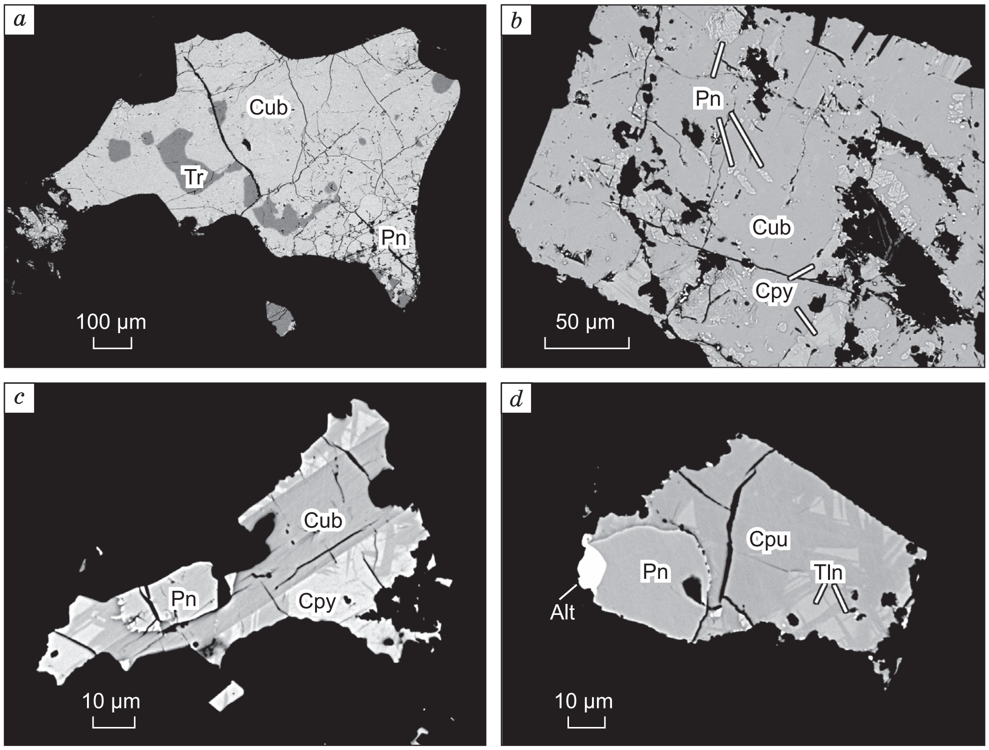

Fig. 5. Products of solid-phase transformations of copper-rich sulfide Ni-Cu-Fe solid solutions: iss_1 → …….. → iss_5 (in reflected electrons, see footnote[3]). *a*, The iss_1 crystal that underwent exsolution into troilite, cubanite, and isolated pentlandite (the D12/15a sample); *b,* a part of the iss_2 crystal represented by the exsolution products including a cubanite matrix and lamellae of chalcopyrite and pentlandite (D12/15a); *c*, the iss_4 small crystal that underwent two-stage exsolution, as a result of which it was transformed into large and small-plate intergrowths of cubanite with chalcopyrite and isolated pentlandite (D11/15a-1); *d*, the altaite grain (PbTe, white), intersecting the boundary between pentlandite and lamellar intergrowths of chalcopyrite and talnahite (lighter) – as the exsolution products of iss_5 (the D12-15a sample).

Morphology and distribution of PGMs by types of the sulfide mineralization are nonuniform.

In sulfide-bearing schlieren from the upper part of the Konnikov Zone, the largest grains > 5–10 μm in size are confined to the contacts of the Ni-Cu-Fe sulfide grains with silicates (Fig. 7*b,d*). Smaller inclusions are observed inside the sulfide phases or in the form of growths into a silicate matrix that is more often represented by the products of secondary changes of olivine and plagioclase (Spiridonov et al., 2019a) – at a certain distance (tens to hundreds of microns) from sulfides (Fig. 7*a*). The most common PGM in these troctolites is a moncheite Pt (Te, Bi)$_2$, which usually forms

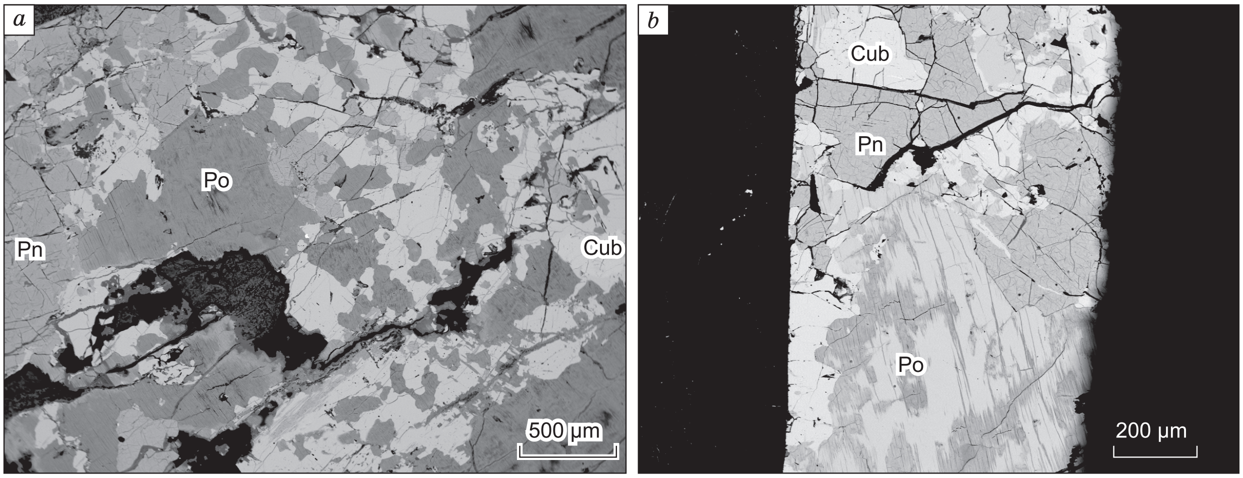

Fig. 6. BSE images of sulfides from the 13DV551-4 pegmatoid troctolite (the 13DV551-4a-2d thin section). *a*, The region of a large mss crystal that underwent exsolution into pyrrhotite, pentlandite (gray), and cubanite (light gray); *b,* sulfides between plagioclase and olivine crystals, carried out by the mss exsolution products.

Table 3. Compositions of the PGE minerals from the sulfide-bearing troctolites of the Konnikov Zone

Component	Lower zone, pegmatoid troctolite 13DV551-4a and 13DV551-1-6*								Upper zone, 13DV554-1 and 13DV554-4				
	1	2	3	4	5	6	7	8	9	10	11	12	13
Pt, wt.%	20.39	22.07	4.26	32.94	0.47	–	36.18	–	34.50	39.00	37.76	37.76	33.53
Pd	8.86	7.95	1.33	0.36	20.96	32.31	0.2	62.76	2.64	–	–	1.16	1.91
Rh	–	–	0.34	–	–	–	–	–	0.47	0.46	0.16	1.17	0.65
Ru	–	–	1.05	–	–	–	–	0.41	0.71	0.35	1.00	0.37	0.71
Ir	–	–	–	–	–	–	–	–	–	1.51	–	–	–
Os	–	–	0.51	–	–	–	–	–	–	–	–	–	–
Ag	0.25	0.27	–	–	0.29	–	0.21	–	–	–	–	–	–
Cu	–	–	–	–	–	–	–	–	–	–	–	0.25	0.63
Ni	–	–	–	–	–	–	–	–	–	0.18	0.26	0.13	0.15
Fe	–	–	–	–	–	–	–	–	–	–	–	–	–
Te	18.97	17.33	33.19	4.5	–	5.63	24.04	1.03	42.06	48.50	39.59	59.67	41.34
Bi	47.09	47.09	8.65	58.62	78.2	58.5	38.75	–	1.92	5.88	1.02	6.16	1.07
Pb	–	–	45.69	–	–	–	–	–	10.33	3.06	10.04	–	10.43
Sn	–	–	–	–	–	–	–	36.6	–	–	–	–	–
Sb	–	–	–	2.15	–	–	–	–	–	–	–	–	–
As	–	–	–	–	0.66	–	–	–	–	–	–	–	–
Hg	–	–	–	–	–	–	–	–	6.98	0.93	9.80	–	8.95
Total	95.56	94.71	95.02	98.57	100.58	96.44	99.38	99.8	99.61	99.87	99.63	99.69	99.37
Number of atoms in the formula													
Pt, un	0.56	0.61	0.08	1.00	0.01	–	0.99	–	0.83	0.93	0.93	0.87	0.81
Pd	0.44	0.41	0.04	0.02	1.01	0.97	0.01	1.96	0.12	–	–	0.06	0.09
Rh	–	–	0.01	–	–	–	–		0.02	0.02	0.01	0.05	0.03
Ru	–	–	0.04	–	–	–	–	0.01	0.03	0.02	0.05	0.02	0.03
Ir	–	–	–	–	–	–	–		–	0.04	–	–	–
Os	–	–	0.01	–	–	–	–		–	–	–	–	–
Ag	0.01	0.01	–	–	0.01	–	0.01		–	–	–	–	–
Cu	–	–	–	–	–	–	–	–	–	–	–	0.01	0.05
Ni	–	–	–	–	–	–	–	–	–	0.01	0.01	0.01	0.01
Fe	–	–	–	–	–	–	–	–	–	–	–	–	–
Te	0.79	0.74	0.91	0.21	–	0.14	1.00	0.03	1.56	1.76	1.50	1.85	1.52
Bi	1.20	1.23	0.14	1.66	1.92	0.89	0.99	–	0.04	0.13	0.02	0.13	0.02
Pb	–	–	0.77	–	–	–	–	–	0.24	0.02	0.23	–	0.23
Sn	–	–	–	–	–	–	–	1.00	–	–	–	–	–
Sb	–	–	–	0.11	–	–	–	–	–	–	–	–	–
As	–	–	–	–	0.05	–	–	–	–	–	–	–	–
Hg	–	–	–	–	–	–	–	–	0.16	0.02	0.24	–	0.21
Total	3	3	2	3	3	2	3	3	3	3	3	3	3

Note. Numbers 1–6 correspond to numbers of PGMs shown in Fig. 8: 1, $(Pt, Pd, Ag)_{1.01}(Te, Bi)_{1.99}$ moncheite; 2 and 3, intergrowth of the $(Pt, Pd, Ag)_{1.03}(Te, Bi)_{1.97}$ moncheite and the $(Pb, PGE)_{0.95}(Te, Bi)_{1.05}$ PGE-containing altaite; 4, $(Pt, Pd)_{1.02}(Bi, Te, Sb)_{1.98}$ insizwaite; 5 and 6, intergrowth of the $(Pd, Pt, Ag)_{1.03}(Bi, Te)_{1.97}$ froodite and $Pd_{0.97}(Bi, Te)_{1.03}$ sobolevskite; 7, $(Pt, Pd, Ag)_{1.01}Bi_{0.99}Te$ maslovite; 8, $(Pd, Ru)_{1.97}(Sn, Te)_{1.03}$ paolovite. Numbers 9–13 correspond to the compositions from Tables 1–3 in (Spiridonov et al., 2019a), where the data for troctolites from the upper part of the Konnikov Zone with disseminated sulfide impregnations are inaccurately represented as "pegmatoid": 9, 3(T) in Table 1; 10 and 11, 5(T) and 6(T) in Table 2; 12 and 13, 7(T) and 8(T) in Table 3.

* From the debris at the point of selection of pegmatoid troctolites in the lower troctolite zone.

irregularly grains, often in intergrowths with kotulskite Pd (Te, Bi) (Fig. 7*a*) and telargpalite $(Pd, Ag)_3Te$ (Fig. 7*c,d*), but less commonly with pentlandite (Fig. 7*b*) and altaite. In polished sections of sample 13DV554-1, the size of the moncheite grains may reach values as large as 30 μm, but usually it is <10 μm. The moncheite composition varies from the almost stoichiometric platinum bitelluride $PtTe_2$ to a complex bivismuthotelluride with an atomic ratio of Te:Bi of about 13. The special feature of the moncheite composition is that tellurium is often substituted not only with bis-

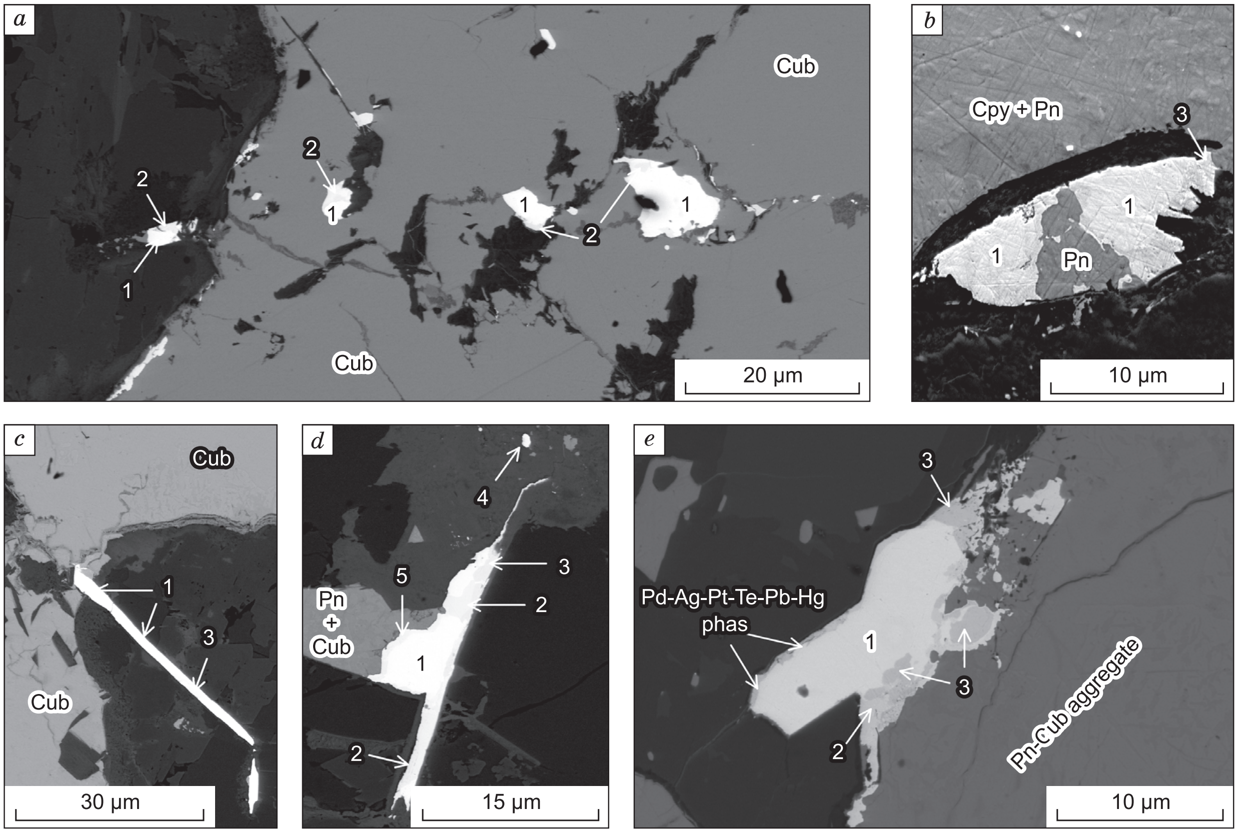

Fig. 7. BSE images of the PGE minerals in sulfide-bearing troctolite from the upper part of the Konnikov Zone (the 13DV554-1-3 and -12 samples) obtained using an ultra-high resolution Hitachi SU-70 FESEM field-emission electron microscope. *a*, The chains of composite grains composed mainly of moncheite (white) and kotulskite (light gray); *b*, splicing of moncheite and pentlandite as crystallization products of the iss solution; *c*, the needle (the cross section of the plate?) of moncheite with inclusions of telargpalite; *d*, the composite grain of moncheite and kotulskite with inclusions of telargpalite and a fragment of tetraferroplatinum; *e*, the large moncheite grain with two rims: a submicron rim of nonstoichiometric (probably heterogeneous) Pd-Ag-Pt-Te-Pb-Hg phase along the boundary with a silicate matrix and a two-phase rim comprised of intergrowths of kotulskite and telargpalite at the contact with the Pn-Cub aggregate. Indexation of the of PGE minerals: 1, moncheite Pt(Te, Bi, Pb, Hg)$_2$, 2, kotulskite Pd(Te, Bi, Pb), 3, telargpalite (Pd, Ag)$_3$(Te, Hg), 4, potarite PdHg, and 5, tetraferroplatinum Pt(Fe, Cu).

muth, but also lead and even mercury (Spiridonov et al. 2019a) (Table 3). The concentrations of both elements can reach 10–12 wt.%. Sometimes platinum dibismuthide $PtBi_2$ (insisvite) associates with moncheite.

The second most abundant PGM is kotulskite Pd (Te, Bi, Pb), represented by separate grains and intergrowths with moncheite, less often with altaite PbTe and paolovite Pd_2Sn. Sometimes there are rims or intergrowths of kotulskite with telargpalite (Fig. 7*e*). As a rule, its size is less than 5–10 μm. Like moncheite in the upper part of the Konnikov Zone, kotulskite contains a lot of lead, which is up to 15–20 wt.%, and the amount of mercury varies from minor fractions to 6.5 wt.% In this case, the ratios of Te and Bi vary widely as the Bi content in individual grains reaches ~17 wt.%. Froodite $PdBi_2$, which is close to a stoichiometric mineral, is also found (up to 7 μm), and it is associated with moncheite and kotulskite, sometimes forming intergrowths with altaite.

The main carriers of silver in the sulfide-bearing troctolites are pentlandite and cubanite (see the section on sulfide geochemistry), and this iss-related association is manifested of telargpalite (Pd, Ag)$_3$Te, which is most typical of the upper part of the Konnikov Zone. Sometimes it is observed in the form of rare isolations in a silicate matrix, but more often as irregularly shaped rims on the periphery or at the contacts of moncheite and kotulskite with Pn–Cub aggregates (Fig. 7*d,e*). At that, grains with traces of lead or grains with none at all predominate, but, in some cases, the Pb content in telargpalite reaches 4 wt.% (Spiridonov et al., 2019a). The mercury content varies from ~1 to 11 wt.% Hg. The image in Fig. 7e is interesting in that a thin rim of an unidentified phase of a complex composition is established at the boundary between a large moncheite grain and a silicate matrix, which comprises ~33 wt.% of Pd, 22 wt.% of Ag, 29 wt.% of Te, 5 wt.% of Pt, 6 wt.% of Pb, and 7 wt.% of Hg. The (Pd + Ag + Pt)/(Te + Pb + Hg) ratio in this phase is about 2, i.e., it is intermediate between telargpalite and kotulskite.

For pegmatoid troctolites, large PGM grains at the edges of sulfides are not typical. Most platinum-metal phases are located inside the sulfide minerals: Pt and Pd bismuthotellurides and bismuthides more often occur at the boundaries

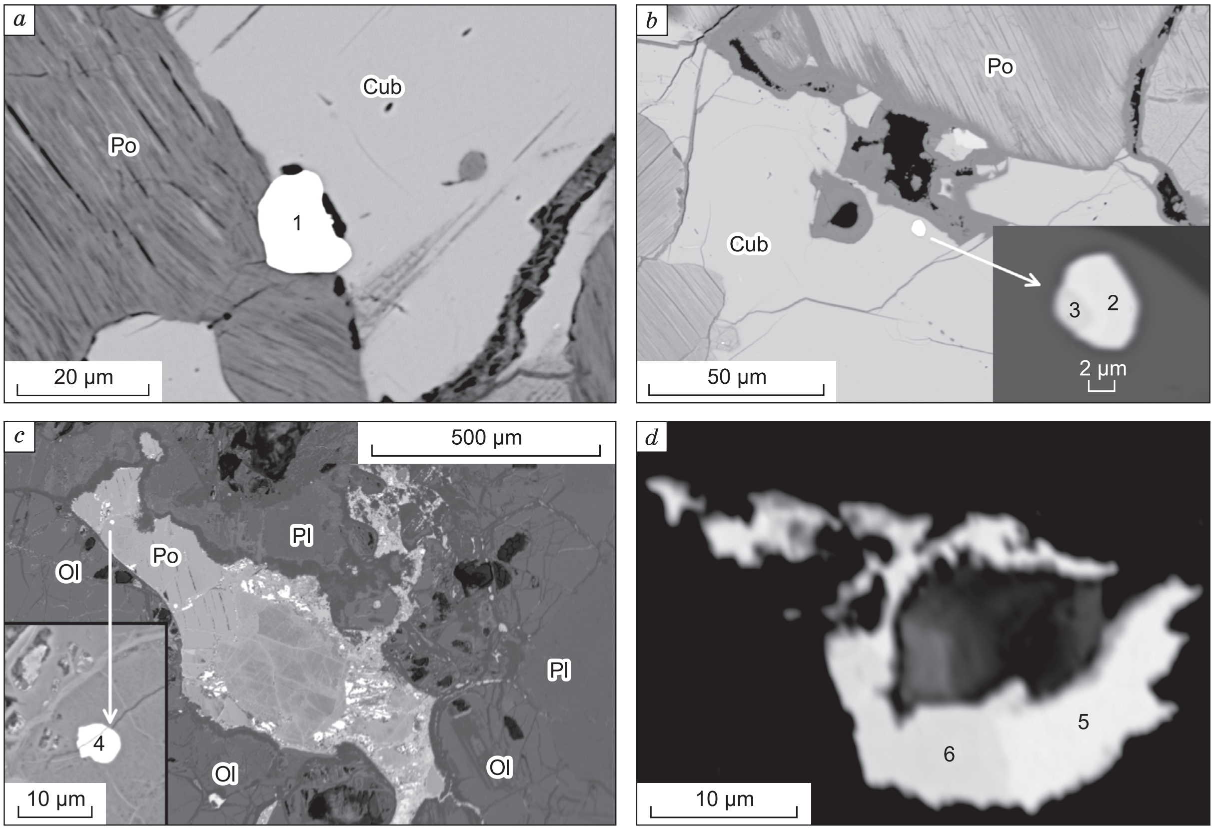

Fig. 8. BSE images of the PGE minerals in sulfide-bearing troctolite from the lower part of the Konnikov Zone (the 13DV551-4a and 13DV551-1-1 samples) obtained using a JSM-6480LV electron microscope. *a,* Moncheite grain (1) at the boundary between pyrrhotite and cubanite; *b,* intergrowth of moncheite (2) and altaite (3) in cubanite; *c,* inclusion of insizwaite Pt $(Bi,Sb)_2$ (4) inside a partially altered pyrrhotite grain; *d,* the composite grain of high-Bi phases in a serpentinite-chlorite matrix from the halo of secondary changes of a large sulfide grain, including froodite $PdBi_2$ (5) and sobolevskite PdBi (6). Indexation of the minerals corresponds to the compositions in Table 3.

of cubanite and pyrrhotite (Fig. 8*a*) or inside cubanite (Fig. 8*b*), and, in two cases, small moncheite grains are observed in pyrrhotite and products of its secondary alteration. Unlike the upper parts of the Konnikov Zone, the mercury content in monchite is usually below the detection limit (Table 3). In the only case, the inclusion of insizwaite $PtBi_2$ in pyrrhotite is established (Fig. 8*c*). Froodite $PdBi_2$ is identified twice in the form of composite grains: as intergrowths with sobolevskite in the serpentine-chlorite matrix of secondary changes in the first case (Fig. 8) and as part of a heterogeneous oval inclusion at the boundary of pyrrhotite and cubanite in the second case, possibly due to immiscibility in the hosting sulfide solution (see “Results and Discussion”). For the main tellurium carriers, which are moncheite (8 grains) and maslovite (4 grains), high Bi/Te ratios are typical, which allows for significantly distinguishing these PGMs from their analogs from the upper part of the Konnikov Zone (Table 3) and emphasizes the “Bi-specialization” of the PGE mineralization. Another characteristic feature of pegmatoid sulfides is a sporadic distribution of small (usually <1–2 µm) grains of paolovite Pd_2Sn, more often in cubanite, but also in pyrrhotite.

Among other sulfide-related phases, altaite PbTe is coming, sometimes occurring as intergrowths with platinum and palladium bismuthotellurides (Fig. 3b). Small (<5 µm) sphalerite grains are often observed in the cubanite matrix and at the boundaries of cubanite and pyrrhotite. The subidiomorphic form of the largest sphalerite crystal 15 µm in size suggests a low-temperature history of post-solidus transformations of the initial sulfide solutions (see “Results and Discussion”). Among unidentified phases in pyrrhotite and products of its secondary alterations, two sulfoarsenide inclusions having a size of <5 µm and containing about 22 wt.% of As, 16–18.8% of S, and ~ 55% of PGEs (Ru + Ir + Os + Rh + Pt) are found. In veins of secondary sulfides, the inclusions of argentite Ag_2S and hessite Ag_2Te are observed, sometimes associating with native silver. In one case, the presence of gold amalgam (Au–Hg) is determined.

GEOCHEMISTRY OF ROCKS AND SULFIDE MINERALS

The bulk concentrations of petrogenic oxides and incompatible trace elements in troctolites are given in Table 4.

The geochemical characteristics of sulfide-bearing species do not differ from ordinary troctolites, which are examined in detail in (Ariskin et al., 2018b). These rocks are characterized by extremely low contents of incompatible elements, often lower than in dunites, and by distinct maxima for Sr and Eu. This fact is evidenc of the relative accumulation of a feldspar component, which is probably due to removal of the intercumulus melt from the protocumulate during its cotectic (Ol + Pl) precrystallization. In the context of the article, the attention is focused on the behavior of chalcogenes

Table 4. The content of petrogenic oxides and incompatible elements in the examined study

Component	1	2	3	4	5	6	7	8	9	10	11	12	13
SiO_2, wt.%	42.50	43.75	41.21	40.71	42.50	41.03	41.66	38.97	40.55	42.72	41.24	42.05	41.07
TiO_2	0.02	0.04	0.04	0.02	0.03	0.02	0.02	0.03	0.03	0.02	0.02	0.02	0.04
Al_2O_3	14.82	21.28	8.14	7.66	15.47	8.27	10.81	13.83	13.27	16.03	8.75	14.76	10.34
FeO	8.35	5.97	11.65	11.87	8.30	11.38	10.40	13.20	12.10	8.26	11.23	9.64	11.60
MnO	0.13	0.09	0.17	0.17	0.12	0.16	0.15	0.12	0.13	0.12	0.16	0.13	0.16
MgO	25.49	15.94	33.29	34.56	24.49	33.87	30.28	22.23	25.22	23.53	33.08	24.66	30.50
CaO	7.80	11.09	4.60	4.11	8.10	4.44	5.72	7.21	6.75	8.32	4.64	7.70	5.38
Na_2O	0.58	1.24	0.36	0.30	0.64	0.31	0.52	0.73	0.61	0.69	0.37	0.59	0.39
K_2O	0.05	0.09	0.03	0.02	0.03	0.03	0.04	0.07	0.05	0.03	0.04	0.04	0.04
P_2O_5	0.01	0.01	0.01	0.01	0.01	0.01	0.01	0.01	0.01	0.01	0.01	0.01	0.01
Cr_2O_3	0.15	0.20	0.34	0.40	0.19	0.38	0.27	0.20	0.25	0.19	0.31	0.17	0.29
NiO	0.10	0.10	0.14	0.15	0.10	0.11	0.13	0.59	0.26	0.08	0.14	0.13	0.16
S	–	0.19	0.01	0.02	0.01	–	0.01	2.82	0.76	–	–	0.09	0.02
Total	100.00	100.00	100.00	100.00	100.00	100.00	100.00	100.00	100.00	100.00	100.00	100.00	100.00
LOI	0.11	1.48	–0.35	–0.06	0.44	–0.06	1.51	1.55	1.19	–0.16	0.37	0.20	<0.05
Li, ppm	1.82	1.70	2.60	2.43	–	2.40	2.80	2.70	2.60	–	2.60	1.90	2.60
Cs	0.009	0.022	0.017	0.050	–	0.045	<0.013	<0.013	<0.013	–	<0.013	<0.013	<0.013
Rb	0.61	1.21	0.80	0.45	0.10	0.38	0.41	0.74	0.34	0.20	0.30	0.25	0.55
Sr	107.3	144.7	60.8	59.8	108.8	61.1	80.0	102.7	93.8	130.6	65.8	90.7	72.6
Ba	22.5	43.0	15.4	12.5	24.5	13.0	18.5	35.7	26.0	20.2	15.2	22.5	16.2
Y	0.42	0.89	0.93	0.24	<1	0.22	0.30	0.48	0.34	<1	0.26	0.36	0.45
Zr	1.32	4.00	2.97	0.67	1.10	1.50	1.50	1.50	<6	1.10	1.50	7.00	7.00
Hf	0.034	<0.14	0.083	0.018	–	<0.14	<0.14	<0.14	<0.14	–	<0.14	0.150	0.160
Nb	0.074	0.186	0.134	0.043	<0.5	0.048	0.059	0.091	0.089	<0.5	0.043	0.065	0.117
Ta	0.010	0.013	0.013	0.008	–	<0.007	<0.007	<0.007	<0.007	–	<0.007	<0.007	<0.007
La	0.619	1.290	0.667	0.260	–	0.310	0.510	1.150	0.770	–	0.360	0.640	0.670
Ce	1.082	2.480	1.291	0.456	–	0.510	0.820	1.880	1.420	–	0.700	1.160	1.290
Pr	0.117	0.259	0.155	0.052	–	0.064	0.106	0.233	0.161	–	0.073	0.134	0.140
Nd	0.438	1.020	0.625	0.197	–	0.220	0.350	0.780	0.610	–	0.260	0.510	0.570
Sm	0.083	0.186	0.141	0.036	–	0.031	0.063	0.129	0.108	–	0.045	0.093	0.098
Eu	0.106	0.160	0.078	0.049	–	0.058	0.077	0.127	0.107	–	0.063	0.098	0.081
Gd	0.075	12.510	0.145	0.032	–	4.930	6.450	8.430	0.079	–	5.430	0.069	0.088
Tb	0.012	0.026	0.025	0.006	–	0.007	0.009	0.017	0.011	–	0.006	0.011	0.015
Dy	0.073	0.150	0.163	0.040	–	0.032	0.049	0.096	0.071	–	0.038	0.066	0.087
Ho	0.016	0.031	0.034	0.010	–	0.008	0.012	0.019	0.014	–	0.009	0.015	0.019
Er	0.046	0.098	0.105	0.029	–	0.033	0.038	0.068	0.045	–	0.035	0.045	0.067
Tm	0.008	0.014	0.017	0.006	–	0.005	0.006	0.009	0.008	–	0.006	0.008	0.009
Yb	0.058	0.085	0.116	0.045	–	0.035	0.051	0.064	0.048	–	0.048	0.048	0.068
Lu	0.010	0.015	0.020	0.008	–	0.008	0.011	0.012	0.008	–	0.011	0.009	0.011
Pb	0.33	2.40	0.32	1.10	–	0.80	0.40	14.40	5.50	–	0.40	0.80	0.70
Th	0.067	0.182	0.133	0.030	–	0.046	0.050	0.052	0.060	–	0.046	0.083	0.074
U	0.010	0.034	0.020	0.006	–	<0.011	0.013	0.013	0.017	–	<0.011	0.011	0.023

Note. The sample numbers correspond to the sequence in Table 1. The contents of the main and impurity elements in nonmineralized troctolites (1, 3, 4) are determined in the analytical laboratory of the University of Tasmania (CODES, Hobart, Australia) – XRF+ICP-MS. The remaining (sulfide-bearing) troctolites were investigated in the GEOLABS laboratory (Ontario, Canada), see explanations for analytical methods.

Table 5. Concentrations of chalcogenes and chalcophile elements in the examined study

Component	1	2	3	4	5	6	7	8	9	10	11	12	13
S, wt.%		0.19	0.01	0.02	0.01	0.003	0.006	2.82	0.76	0.003		0.09	0.02
Se, ppm	<0.4	0.70	<0.4	<0.4		<0.4	<0.4	5.90	1.50		<0.4	<0.4	<0.4
Te	<0.05	0.49	<0.05	<0.05		0.05	0.04	0.69	0.29		0.03	0.21	0.16
Zn	47	76	58	59	48	71	70	163	63	48	72	54	69
Cu	9	1084	20	30	73	34	33	3335	1240	9	5	486	372
Co	754	814	1138	1143	805	863	1022	4668	2000	641	1105	1011	1229
Ni	101	80	133	150	100	159	136	267	153	99	147	105	133
Mo	0.019	0.090	0.015	0.015		0.080	0.060	0.120	0.260		0.070	0.330	0.170
Ag		0.31				0.03	0.02	1.74	0.73		0.01	0.15	0.11
Cd	0.008	0.065	0.011	0.020		0.024	0.027	0.453	0.301		0.031	0.036	0.037
Sn	0.032	0.330	0.043	0.272		0.210	0.340	0.820	0.410		0.210	<0.16	0.200
Pb	0.33	2.40	0.32	1.10		0.80	0.40	14.40	5.50		0.40	0.80	0.70
Au, ppb		40.0				<0.4	1.2	63.1	7.5		0.4	31.3	23.4
Ir		7.3				3.3	5.6	8.5	6.3		5.9	8.6	7.8
Pd		138.0				4.5	13.7	252.0	89.1		13.3	232.0	136.0
Pt		188.0				6.0	11.8	189.0	63.7		26.4	182.0	117.0
Rh		12.5				2.3	2.2	8.5	5.8		1.7	10.5	8.3
Ru		12.9				9.8	9.7	10.2	8.0		8.5	7.9	11.5
S/Te		3857				600	1500	40884	26335		1000	4318	1254
S/Se		2700						4781	5091				

Note. The sample numbers correspond to the sequence in Tables 1 and 4.

and a number of chalcophile elements, and their concentrations, including PGE, are given in Table 5. These data show that the highest concentrations of sulfur correspond to increased concentrations of Se and Te. This allows one to consider chalcogenes as an indicator of the degree of sulfide accumulation, which is convenient for constructing plots that indicate a relationship between the PGE concentration and the amount of sulfide phases (Ariskin et al., 2018c). Similar relationships are shown in Fig. 9, which shows positive correlations of the Pd, Pt, Au, and Cu concentrations as a function of the total tellurium content.

The sublinear character of these relationships is due to the fact that the compositions of various types of rocks (including troctolites) and ores of Dovyren form a single trend linking the compositions of model protosulfide liquids (red asterisk in Fig. 9) and chilled rocks from the basement of the intrusion. Instead of a direct genetic relationship (which would be odd for rocks distanced at nearly 1.5 km by stratigraphic levels), this suggests a common geochemical source, i.e., the Dovyren magma and the same laws of its differentiation during the formation, migration, and evolution of immiscible sulfides. At the same time, it is interesting that, similarly to the data for sulfide-bearing ultramafics of Dovyren (Ariskin et al., 2018c), the apparent correlation between the Au and Te concentrations clearly points to a sulfide precursor, whose initial components also included gold rather than simply platinum and copper. The same data demonstrate an obvious paradox as the composition of quenched picrodolerite, which includes a primitive sulfide material by definition (a green asterisk in Fig. 9), is close to the composition of troctolites with sulfide mineralization of a high-copper type, i.e., the sulfides representing the latest and low-temperature stages of evolution of the iss solutions (Fig. 5). A physicochemical interpretation of this contradiction is given in the discussion of the results.

Meaning of S/Se and Se/Te ratios in rocks. The interval of mantle values of the S/Se ratio (2850–4350) is traditionally used to determine mineralized rocks and sulfide phases that have retained the signature of their primary mantle origin (Queffurs and Barnes, 2015; Holwell et al., 2015). It has been assumed that the increased ratios S/Se > 4350 may indicate contamination of crustal rocks, and relatively low values of S/Se <2850 are the result of sulfur loss in post-magmatic processes (Smith et al., 2016). Data for sulfide-bearing troctolites demonstrate boundary values that most likely indicate a mantle source with a low contribution of the contaminated component and an insignificant role of over-printing processes (Table 5). In this case, an alternative mechanism for increasing S/Se in sulfides and mineralized rocks should be taken into account, which is related to the possibility of significant extraction of selenium by a sulfide liquid from the silicate magma ($D_i^{Sf/Melt}$ for selenium is about 1500 (Smith et al., 2016)) with progressing silicate-sulfide immiscibility.

Wide variations of the S/Te ratios (Table 5) can be considered as further evidence for the evolution of a protosulfide material. Assuming that there is 19.3 ppm of Te and 35.5 wt.% of S in the initial sulfide (Ariskin et al., 2018c),

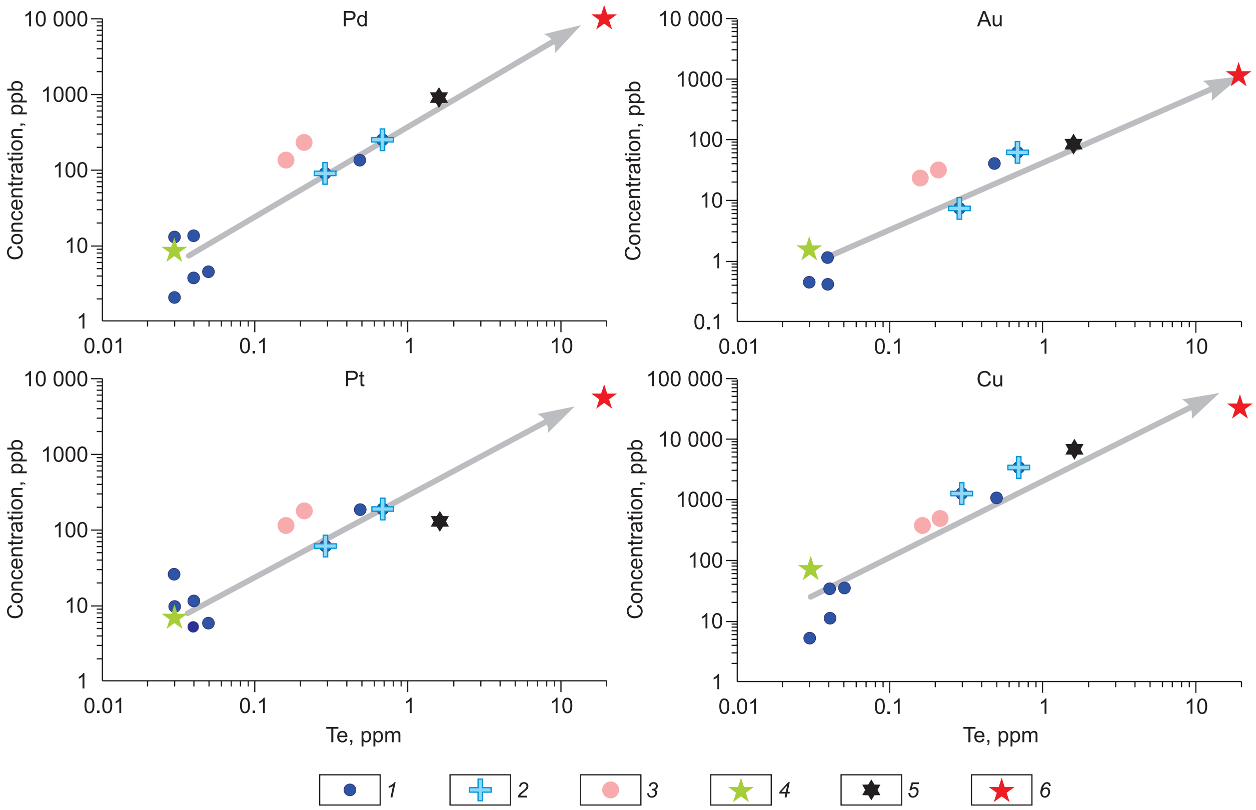

Fig. 9. Concentrations of light platinoids (PPGE), Au, and Cu versus the total content of tellurium. The blue and pink colors refer to the lower and upper parts of the Konnikov Zone, respectively: *1*, rocks with disseminated copper-rich sulfides, *2*, pegmatoid troctolites, and *3,* the 13DV554-1 and 13DV554-4 samples (Nos. 12 and 13 in Table 4). The data of (Ariskin et al., 2018c) are shown for comparison: picrodolerite (4) represents a primitive rock from the chilled zone (the DV30-1 sample), the net-textured ore (5) refers to the 07DV107-1 sample, and the "initial sulfide" *6* stands for the estimate of the origianl immiscible sulfide liquid using the COMAGMAT-5 software, which corresponds to 88% crystallization of the primitive DV30-2 orthocumulate at a temperature of 1125 °C and a sulfide content of 0.13 wt.%.

the 18394 ratio is calculated. The characteristics of samples 13DV551-4a and -4e are the closest to this estimate (columns 8 and 9 in Table 5). They represent rocks from the lower part of the Konnikov zone, containing maximum amounts of the exsolution products of a monosulfide solution: from 60 to 77% of pyrrhotite (± troilite) and pentlandite (Table 2). Other troctolites with copper-rich sulfide mineralization manifest low values of S/Te in a range from 600 to 4318. Thus, the troctolites are divided into two groups relative to the assumed initial sulfide: 1) rocks with a 1.4-2.1-fold increase in the S/Te and 2) those with sharply lower S/Te ratios. Such relationships correspond to the laws of crystallization of sulfide solutions as the restite mss associations are depleted in light PGE and Te during the complementary enrichment in these elements at the crystallization front of the residual, more cuprous sulfide liquid (Helmy et al., 2007; Holwell and McDonald, 2007; Distler et al., 2016; Sinyakova et al., 2017, 2019).

Geochemistry of sulfide phases. In search for additional arguments for the geochemical evolution and possible spatial separation of the fractions of protosulfide liquids, the trace-element composition of the main sulfide minerals from troctolites was determined. Six samples were studied by the LA-ICP-MS method: D8/15, D12/15, 13DV551-4, 13DV554-1-3, and -1-12, as well as additional mounts for sample 07DV403-1. A total of 148 analyses were obtained (Po – 30, Pn – 43, Cpy – 20, and Cub – 55) for the base metals (Fe, Ni, Cu, and Co) and 17 trace elements (Os, Ir, Ru, Rh, Pt, Pd, Au , Ag, Re, Zn, Cd, Mo, Pb, Bi, Sb, Se, and Te).

The complexity of such studies is due to the phase heterogeneity of sulfide grains as single crystals are rarely tested in the case of sequential evaporation of sulfide material and a laser beam diameter of 22–40 μm. Nevertheless, controlling the ratios of the base metals (Fe/Ni for pentlandite and Cu/Fe for chalcopyrite and cubanite), one can determine the degree of homogeneity and obtain reliable concentrations in each sulfide phase, with more details available in (Ariskin et al., 2016). On the other hand, the object of the research is the exsolution products of mss and iss solutions, which (depending on subsolidus transformations) can demonstrate a wide range of compositions with respect to the main components for the same mineral phase. This is manifested in Fe/Ni variations in the study of pentlandite – 1.50 ± 0.30 on average. Similarly, the term "cubanite" stands for sulfides usually containing <0.5 wt.% of Ni, with parameters being close to $CuFe_2S_3$ (~0.5 of Cu/Fe by weight) and a

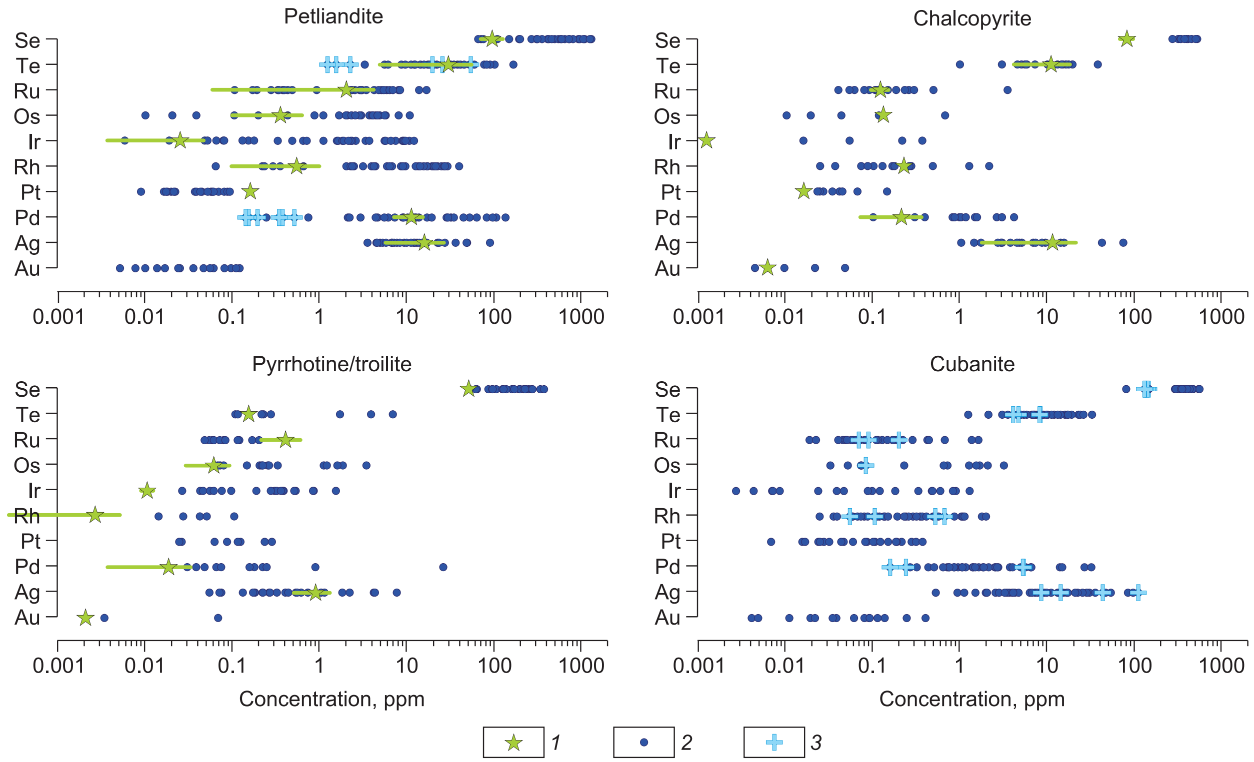

Fig. 10. Concentrations of chalcogenes, PGEs, Ag, and Au in sulfide minerals from picrodolerite and studied troctolites. The data of the LA-ICP-MS analyses for the DV30-1 picrodolerite (1) (Ariskin et al., 2018c) and troctolites with disseminated (07DV403-1, D8/15, D12/15, 13DV554-1-3, and -12) (2) and pegmatoid (13DV551-4) (3) sulfides.

nonstoichiometric, often microheterogeneous phase with the Cu/Fe ratios increased up to ~0.7. In the case of chalcopyrite, the phases of a more uniform composition with Cu/Fe~1 are determined. For the mss exsolution products (a mixture of pyrrhotite and troilite), iron (about 63.5 wt.%) sharply prevails in the composition of the evaporated material, while the total content (Ni + Cu) does not exceed 1 wt.%. Figure 10 presents all data on the concentration of chalcogenes, PGEs, Ag, and Au in sulfide phases from the studied troctolites, and, for comparison, the compositions of primitive sulfides from the picrodolerite of the chilled zone are shown (Ariskin et al., 2018c).

These results confirm the observation that the maximum concentrations of Os, Ir, Ru, Rh, Pd, and Te in sulfides from layered intrusions are typical for pentlandite (Barnes et al., 2008). In the case of Ag and Se, there are comparable concentrations of these elements in pentlandite and cubanite, while the Pt and Au concentrations in all sulfide grains rarely exceed 0.01 ppm (Fig. 10), more often lower than their detection limit. The same pattern is typical for the distribution of platinum and gold in sulfides from ultramafic rocks of the basal zone and chilled rocks of the Yoko-Dovyren intrusion (Ariskin et al., 2016, 2018c) (Fig. 10, condition *1*). Taking into account the sulfide control of these elements in troctolites (Fig. 9), we attribute such relationships to segregations of the main mass of platinum in the form of moncheite (Figs. 7, 8), and Au with submicron precipitates of a high-grade electrum.

When comparing data for cubanite and pentlandite, one may observe another interesting phenomenon. For cubanite, the concentrations of noble metals and chalcogenes overlap in the iss and mss crystallization products (Fig. 10, condition *3*). For pentlandite, the Te and Pd distribution is bimodal: the minimum contents of these elements are characteristic of the pegmatoid sulfides as mss derivatives, and these variations reach from two to three orders of magnitude. This fact is consistent with the conclusion based on the analysis of S/Te ratios in troctolites, stating that the mss associations of the pegmatoid sulfides are generally depleted of Pd and Te as compared to the exsolution products of iss sulfide solutions. This is more clearly shown in comparing the average compositions of pentlandite in each of the samples in Table 6 and Fig. 11, in which these variations are shown as a function of rhodium concentration.

The choice of rhodium as an indicator of the evolution of the composition of pentlandite (as the main host of noble metals during the evolution of mss and iss solutions) is explained by the absence of its own phases in sulfide-bearing troctolites and the sequential enrichment of more cuprous fractions of sulfides (Fig. 11). This behavior is consistent with experimental results (Mungall, 2005), which predict a sharp decrease in the partition coefficient of Rh between mss

Table 6. Compositions of pentlandite in picrodolerite and in the studied samples of sulfide-bearing troctolites from the Konnikov zone

Sample	DV30-1 [7]	D12/15 [6]	07DV403-1 [7]	D8/15 [2]	13DV551-4a [6]	13DV554-1-3 [12]	13DV554-1-12 [10]
Fe, wt.%	35.22 (2.17)	37.23 (0.64)	39.38 (0.75)	36.14 (1.29)	34.82 (1.12)	39.92 (1.59)	39.70 (2.81)
Ni	27.35 (2.38)	24.71 (1.16)	24.57 (2.00)	24.96 (0.14)	27.94 (1.29)	22.60 (1.97)	22.21 (2.99)
Cu	0.07 (0.13)	1.24 (0.96)	0.42 (0.29)	1.92 (1.43)	0.10 (0.17)	0.42 (0.85)	1.11 (1.75)
Co	1.39 (0.27)	0.84 (0.07)	1.01 (0.35)	1.02 (0.24)	1.18 (0.13)	1.02 (0.15)	0.96 (0.24)
S*	35.96	35.97	34.62	35.96	35.96	36.04	36.02
Se, ppm	95.6 (26.5)	530 (171)	423 (86)	232 (54)	111 (53)	849 (277)	654 (272)
Te	30.0 (34.7)	66 (37)	31 (29)	46 (12)	17 (21)	43 (45)	27 (20)
Zn	2.4 (3.7)	21 (16)	1.8 (2.2)	289 (248)**	4.7 (3.1)	3.6 (2.9)	5.5 (4.7)
Mo	0.02 (0.02)	0.21 (0.13)	9.1 (13.3)	0.12	0.8 (0.5)	1.1 (1.7)	5.8 (13.7)
Ag	16.0 (10.2)	10.6 (4.8)	11.5 (3.7)	27.2	14.7 (6.3)	17.8 (24.1)	19.6 (16.8)
Cd	0.01 (0.01)	2.0 (1.2)	0.19 (0.09)	7.4 (4.9)	1.8 (0.6)	1.9 (1.0)	1.1 (0.9)
Sb	0.13 (0.12)	0.39	n/a	n/a	n/a	n/a	n/a
Pb	5.1 (3.9)	14.9 (9.1)	3.8 (3.2)	80 (58)**	12.3 (5.7)	28.86	19.8 (19.2)
Os	0.36 (0.26)	2.0 (2.4)	2.8 (1.9)	1.4 (0.4)	n/a	4.2 (3.3)	2.7 (1.8)
Ir	0.021 (0.022)	0.67 (0.79)	1.7 (0.8)	1.3 (0.8)	0.12 (0.05)	6.7 (4.0)	3.8 (3.8)
Ru	2.0 (2.0)	2.9 (3.2)	1.8 (1.6)	3.7(1.6)	0.38 (0.04)	7.6 (4.7)	3.6 (2.4)
Rh	0.67 (0.90)	2.2 (1.0)	8.0 (4.2)	3.4 (1.4)	1.0 (1.6)	23.1 (7.2)	11.1 (8.8)
Pd	11.3 (4.1)	5.2 (4.9)	64 (50)	10.1 (4.0)	0.29 (0.15)	34 (29)	19 (33)
Pt	0.054	0.06 (0.01)	0.08	0.09	n/a	0.04 (0.02)	0.04 (0.03)
Au	n/a	n/a	0.04	n/a	»	0.04 (0.04)	0.05 (0.04)

Note. The compositions of pentandite are determined by the LA-ICP-MS method at the University of Tasmania (see the text); the data for the DV30-1 picrodolerite are in Table 4 in (Ariskin et al., 2018c). The number of analyses are in square brackets, and the standard deviations (1σ) are in parentheses; their absence denotes the uniqueness of the measurement; n/a, not available (below detection limit).

*By difference from 100%.

** Probably inclusions of sphalerite and galenite.

and residual sulfide under conditions below QFM in model systems. Experimental measurements of the intrinsic oxygen fugacity in olivine from the Dovyren cumulates indicate an interval below QFM, to about QFM-2.5 (Ariskin et al., 2017b).

Figure 11 shows that, in the case of Se, Pd, Ru, and Ir, there is distinct positive covariance with rhodium and the minimum contents are typical of pegmatoid Fe–Ni sulfides (sample 13DV551-4a), whereas the maximum contents are typical of copper copper-rich sulfide assemblages from the upper part of the Konnikov Zone (samples 13DV554-1-3 and -12). The pentlandite composition of the mss association from the lower part of the Konnikov Zone on average is close to pentlandite, which represents primitive sulfides from the chilled zone (DV30-1, Table 6). In the case of tellurium, this covariance is violated, apparently, due to the formation of moncheite Pt (Te, Bi)$_2$, which is observed at the periphery and inside sulfide grains (Figs. 7, 8). Probably for the same reason, there are no signs of the enrichment in silver in pentlandite as telargpalite (Pd, Ag)$_3$Te (along with kotulskite) in the upper part of the Konnikov Zone usually accompanies moncheite segregations.

RESULTS AND DISCUSSION

The problem of the formation of a localized (in separate regions) or lateral (“reefs”) PGE mineralization in layered intrusions is reduced to two main issues. First, the phase nature of the noble metal concentrator capable of transporting and depositing platinum, gold, and silver in quantities exceeding their content in the parental magmas by thousands times. Second, the physical mechanism of transfer and concentration of this PGE carrier in cumulate rocks. Two concepts are discussed in the ore formation theory, with the presence of sulfide assumed to play an important role in both. This is due to the mineralogy of rocks hosting PGE reefs, whose common feature is low-sulfide mineralization (Maier, 2005).

The first hypothesis assumes the extraction of PGEs from magma by sulfide liquids, which result from the silicate-sulfide immiscibility (Campbell and Naldrett, 1979; Naldrett, 2004) and, under the effect of gravity, can move downward, being accumulated into layers of partially crystallized cumulates (Godel, 2015; O’Driscoll and González-Jiménez, 2016). An alternative takes shape in the 1990s after (Boudreau and McCallum 1992a,b), in which the authors

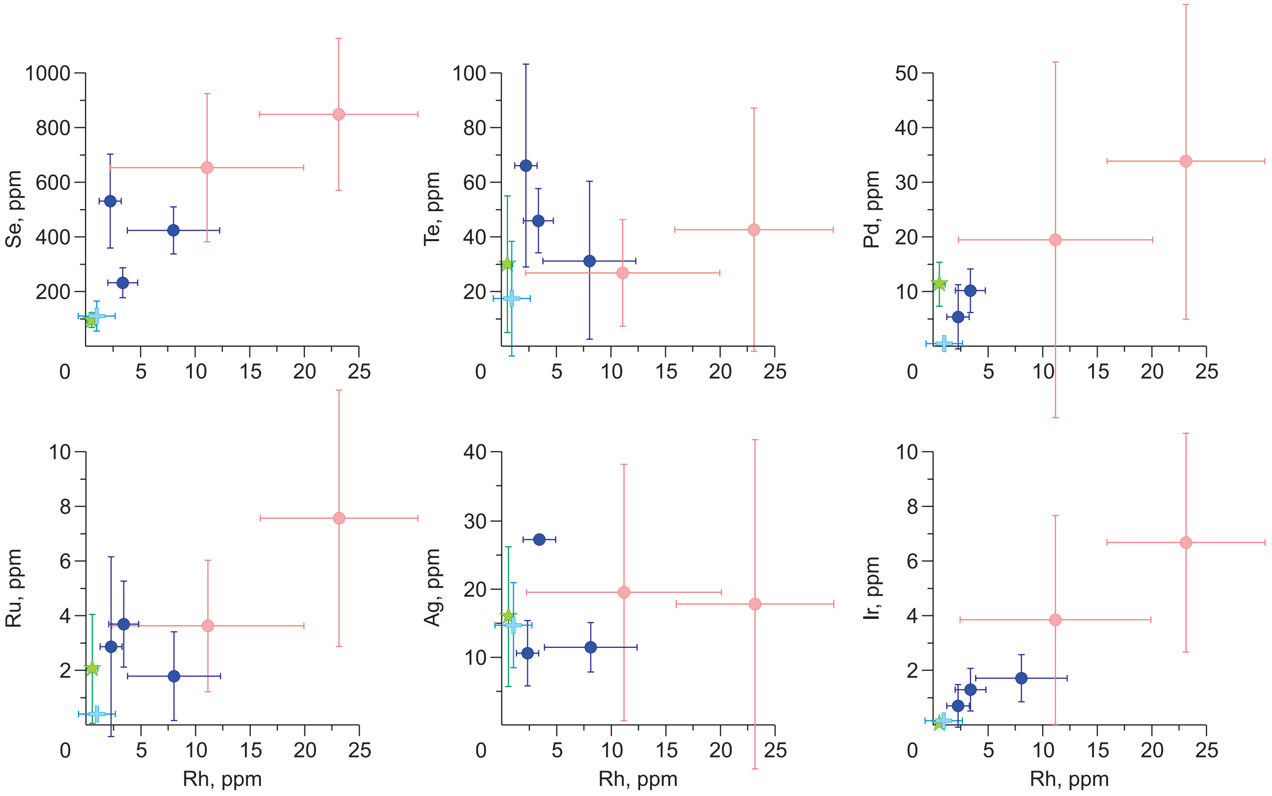

Fig. 11. Concentrations of chalcogenes, PGEs, and silver versus rhodium in pentlandite from picrodolerite and the troctolites studied. See denotations in Fig. 9. The data of LA-ICP-MS analyses are from Table 6. The span of the colored lines corresponds to standard deviations (1σ).

allow for the possibility of dissolution of PGE-containing sulfides by late chlorine- and water-containing fluid and its upward migration, followed by redeposition of the enriched sulfide substance at the fluid saturation front. The main given arguments are usually the ability of PGEs to form stable chloride complexes, the presence of Cl-apatite, and the detection of Cl-containing inclusions in minerals from some ore-bearing complexes.

The problem is that elevated chlorine contents in the samples are usually confined to the upper parts and contacts of the layered intrusions, where they correlate with the maximum amount of intercumulus melt and the enrichment in other incompatible components (Cawthorn, 1994; Barkov and Nikiforov, 2015). The ultra-depletion of the troctolites of Dovyren in REE, Y, Zr, Hf, Ti, P, U, Th, Ba, and Rb (Ariskin et al., 2018b) indicates extremely low porosity of the cumulates and possible depletion in chlorine. This explains why no Cl-apatite grains have been found in these adcumulates (including sulfide-bearing ones). For this reason, the idea that sulfides and PGEs are transferred by Cl-containing fluids through the mass of troctolites seems unlikely. On the contrary, it is observed that these rocks preserve only traces of the strongly reduced light gases H_2, CH_4, and CO (Orsoev, 2019; Konnikov et al., 2000), while the accumulation of relatively heavy volatile components, including Se, Te, Mo, and other elements with chalcophile properties (Sn, Pb, Cd, Ag, Au, and platinoids, Table 5) is observed in the sulfide-bearing varieties.

Considering the schlieren shape of segregations with disseminated sulfides (Fig. 2), the poikilitic structure of the pegmatoid veins (Fig. 3), and the insignificant presence of secondary hydrosilicates (LOI, Table 4), it can be concluded that the mineralization of troctolites gives an example of "pure" sulfide accumulation when there is no need to suggest large-scale fluid transfer. This does not mean that reactions involving fluids play no role in the subsequent evolution of sulfide-bearing cumulates. It is assumed that the components dissolved in a sulfide substance (including some water) have a local effect on the variety of products of low-temperature transformations of subsolidus exsolution products, especially along the periphery of protosulfide agglomerations during their *in situ* crystallization. This interpretation of the phenomenon allows one to abandon superimposed and additional factors and, as applied to sulfide-bearing troctolites, to focus on the parameters of the formation and evolution of the initial sulfide liquids in the strata of crystallizing troctolite cumulates.

Interpretation of sulfide control lines. The fact that the maximum concentrations of chalcogenes in troctolites correspond to the maximum bulk contents of sulfur (Table 5), and the Pd, Pt, Au, and Cu concentrations correlate with tellurium (Fig. 9), indicates that the observed distribution of precious metals is controlled by the amount of sulfides. The consequence of this is the positive covariation of platinum and copper, which is traditionally considered as characteristic relationships, particularly Cu/Pd versus Pd (Naldrett, 2004). The sublinear character of these trends can be easily explained as a result of the monotonous evolution of the sulfide composition in processes of silicate-sulfide immiscibility, according to the law resulting from the consideration of the silicate melt—sulfide liquid binary system (Campbell, Naldrett, 1979):

$$Y_i^{Sf} = X_i^{Magma} D_i^{Sf/Melt} \frac{R+1}{R + D_i^{Sf/Melt}}. \qquad (1)$$

Here Y_i^{Sf} and X_i^{Magma} denote the contents of the *i*th element in the sulfide and original magma, $D_i^{Sf/Melt}$ is the equilibrium partition coefficient in the sulfide-melt system, and *R* is the so-called *R*-factor equal to the ratio of the melt (magma) mass f_{Melt} to the amount of the released sulfide phase f_{Sf}, i.e., $R = f_{Melt}/f_{Sf}$. In this case, any point on the curves of the natural dependence of Cu/Pd on Pd is interpreted as a product of successive depletion of sulfides in Pd and Cu, but at a different rate because the partition coefficients of Pd between the sulfide and melt are 1.5–2.0 orders of magnitude higher than those for copper (Mungall and Brenan, 2014). Graphic reconstructions using the *R*-factor are given in hundreds of publications and for several decades have been considered as fundamentals for the interpretation of the geochemical trends for mineralized rocks and the grade of sulfide ores.

Ariskin et al. (2017a) noticed that this approach was not applicable to systems that are initially undersaturated with respect to sulfide, and, in the case of manifestation of silicate-sulfide immiscibility in the intercumulus melt, one had to account for the number of crystals and the proportion of sulfide precipitates relative to other mineral phases. In the general case, the equation for the evolution of the sulfide composition in a multiply saturated system has the form

$$Y_i^{Sf} = X_i^{Magma} D_i^{Sf/Melt} \frac{(R+1)}{(R + D_i^{Sf/Melt})(1 - f_{Crys})}, \qquad (2)$$

where f_{Crys} is the total fraction of silicate phases and oxides crystallizing in a heterogeneous mixture of rock-forming minerals, immiscible sulfides, and the residual melt. The correct solution to this problem involves the use of algorithms allowing one to simulate different stages of sulfide liquation during sequential crystallization of the parental magmas and primitive cumulates (Ariskin et al., 2018a).

Bimodality of sulfide compositions. In the case of sulfide-bearing troctolites from Dovyren, the concept of the consistently evolving composition of immiscible sulfide liquids encounters a clear contradiction. The whole-rock composition of picrodolerite with primitive sulfides (Ariskin et al., 2018c) for all five elements in Fig. 9 practically coincides with the rocks, including disseminated mineralization with a predominance of copper-rich sulfides. And, on the contrary, the pegmatoid sulfides extremely depleted in PGMs (with predominance of mss products (Fig. 8)) are close to troctolites from the upper part of the Konnikov Zone, bearing more cuprous sulfides and various PGE mineralization (Fig. 7). This is due to the different amounts of sulfide material in the studied samples. Figure 12 shows the same data recalculated for 100% sulfide mass according to the scheme (Ariskin et al., 2018c).

These relationships show that the averaged sulfide material of troctolites is divided into two contrasting groups by composition: those sharply depleted in platinum, Au, Cu, and Te, and those with 10–50-fold enrichment in them. Moreover, the former are somewhat poorer in chalcophile elements as compared with the predicted composition of the most primitive sulfide (red asterisk in Fig. 12), while the latter are noticeably richer. This suggests a limited scale of fractionation of immiscible sulfides as the troctolite cumulates crystallize and that one should look for the causes of such contrasting differences in the post-liquation and, probably, subsolidus evolution of the initial sulfide systems. This is indicated by the peculiarities of the sulfide mineralogy, which allow attributing the group of sulfides most depleted in PGE to the mss crystallization products and the group of sulfides enriched in platinoids and gold to the relatively late iss-type derivatives (Figs. 5, 6). This conclusion is supported by the data of LA-ICP-MS studies of the trace-element composition of sulfide phases (Figs. 10, 11).

Thus, the combination of mineralogical features and geochemical signatures corresponds to the well-known laws of evolution of multicomponent sulfide melts, whose successive crystallization yields a monosulfide solution and a series of lower-temperature solutions, producing residual systems that are more cuprous and richer in PGE (Helmy et al., 2007; Holwell and McDonald, 2007; Distler et al., 2016; Sinyakova et al., 2017, 2019). Interestingly, the S/Se ratios close to the mantle ones and the abnormally high S/Te ratios in pegmatoid troctolites rich in mss products (column 8 in Table 5) are consistent with experimentally established variations of the Se/Te ratio upon crystallization of mss solutions (Helmy et al., 2010; Brenan, 2015).

Evolution of sulfide solutions and the formation of PGMs. The proposed scheme for the post-liquation evolution of the protosulfide material has obvious consequences with respect to platinum metal and other minerals, which precipitate at different stages of crystallization and subsolidus transformation of mss and iss solutions. At the same time, the orthomagmatic history of sulfides sets a geochemical background that predetermines not only the formation and subsequent changes in the phase composition of Cu–Ni–Fe-sulfide assemblages, but also the variety of PGE mineralization. Four main stages are distinguished:

1. Nucleation and agglomeration of the first immiscible sulfide globules in the intergranular space of crystallizing cumulates at temperatures slightly above 1200 °C – see the calculations using the COMAGMAT-5 software (Ariskin et

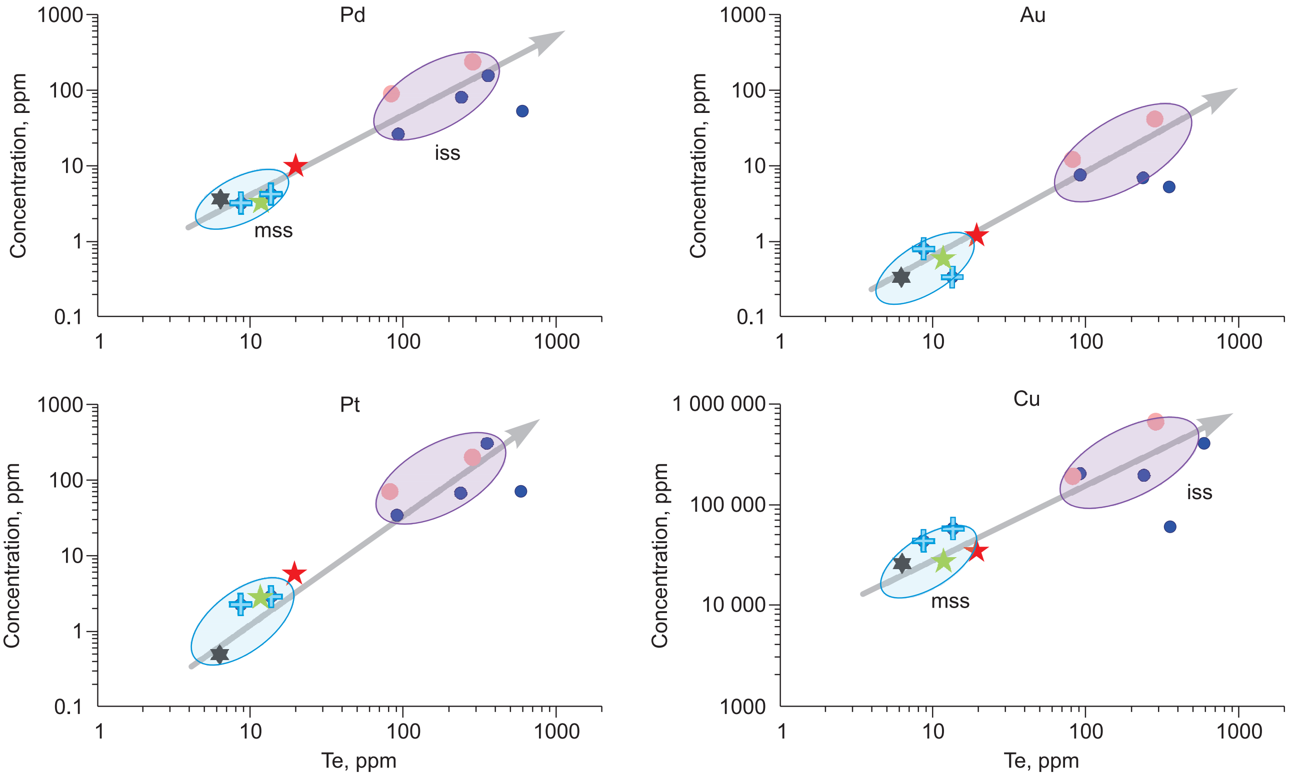

Fig. 12. Normalized concentrations of light platinum metals (PPGE), Au, and Cu versus the normalized tellurium content. See denotations in Fig. 9. Normalization is carried out by recalculating the whole-rock concentrations of the elements per 100% sulfide mass, while the initial sulfide is an estimate of the composition of the most primitive sulfide liquid obtained from the calculations using the COMAGMAT-5 software (Ariskin et al., 2018a,c).

al., 2018c). At this stage, the primary extraction of noble metals and chalcogenes from intercumulus melts proceeds.

2. Downward migration of the protosulfide segregations as the olivine-plagioclase cumulates solidify, probably according to the mechanism of extrusion of the intercumulus pore melt under the effect of gravity (Chung ans Mungall, 2009). This stage implies no significant exchange of precious metals between the sulfide phase and the silicate substance if the underlying cumulus layers have already passed the stage of silicate-sulfide immiscibility.

3. Accumulation of large segregations at the front of critically low porosity in the lower part of the troctolite zone and the onset of crystallization of the monosulfide solution at near-solidus temperatures, probably below ~1100 °C (Kullerud et al., 1969). Accordingly, the fractionation of the residual sulfides along the line of enrichment in Cu, PGE, Au, Ag, and chalcogenes.

4. Spatial separation of the mss restite and complementary sulfide liquids, probably under conditions of the widest possible stability field of the mss + iss + sulfide melt tie-line association at ~900–820 °C (Craig and Kullerud, 1968; Tsujimura and Kitakaze, 2004), i.e., at temperatures 150–200 °C below the dry solidus of troctolites consistent with a gabbronorite melt saturated with olivine and plagioclase (Ariskin et al., 2017a). This process could occur through the percolation of highly cuprous and PGE rich fractions at the latest stages of cumulus solidification — via contraction cracks and micro-pore channels, following with the formation of heterogeneous schlieren and the nests of sulfide material in the troctolite matrix (Fig. 2).

The further history of primary sulfide associations includes subsolidus reactions and a series of polyphase exsolutions of mss and iss solutions. The upper limit of these transformations corresponds to temperatures of about 800 °C, which are consistent with the minimum temperatures of equilibrium crystallization of melts in synthetic Cu-Ni-Fe sulfide systems (Craig and Kullerud, 1968; Tsujimura and Kitakaze, 2004). The fractional crystallization of sulfide melts may result in even lower-temperature derivatives, including a bornite-tss eutectic at a temperature of about 580 °C, where tss is the matrix of the ~$Fe_{21}Ni_{24}Cu_{10}S_{45}$ composition (Sinyova et al., 2018). Judging by the presence of violarite ($FeNi_2S_4$) and pyrite, the record of subsolidus transformations in pegmatoid sulfides can be traced to temperatures of 450–250 °C (Craig, 1971, 1973). In the case of disseminated mineralization rich in copper sulfides, the typomorphic phase is talnachite $Cu_9Fe_8S_{16}$, which (in the Cu-Fe-S system) represents the iss exsolution product at 520 °C (Cabri, 1973) and transforms into other polymorphs at temperatures below 230 °C (Raghavan, 2004). Thus, the possible temperature range for the formation of noble metal mineralization associated with sulfides can be divided into two stages conjugated with (1) the origin and crystallization of immiscible sulfide liquids (~1100–800 °C, possibly slightly lower) and (2) post-solid transformation of the sulfide phases (mss, iss, and their exsolution products) in the course of cooling of the hosting cumulates at temperatures from about 800 to 250 °C.

An alternative point of view is stated by E.M. Spiridonov who believes that most noble metal minerals (Pd, Pt, Au, and Ag) including chalcogenes (± Sn, As, Sb, and Ge) and post-magmatic intermetallic compounds represent pneumatolytic-metasomatic formations at the contacts of sulfide grains and inside the silicate matrix, with the participation of fluids expelled from crystallizing Fe–Cu–Ni-sulfide liquids (Spiridonov et al., 2019a,b). This viewpoint is not shared by all the co-authors of the mentioned publications as the "metasomatic" hypothesis encounters a number of difficulties with respect to the Dovyren troctolites. First, the possibility of metasomatic reactions that could lead to the formation of submicron inclusions and relatively large grains of PGMs directly inside sulfides is open for discussion (Figs. 7*a*, 8*a-c*). Second, it is difficult to attribute almost binary mixtures of cumulus olivine and plagioclase (which make up 97–99% of troctolite volume) to the "silicate matrix" (Table 1). In this case, the phantom nature of the fluids that have not left any significant traces in the mineralogy of these adcumulates should be assumed. In addition, it is doubtful that metasomatic processes can explain a narrow range of the geochemical characteristics of the selected types of sulfide compositions, which correspond to the crystallization laws of Cu–Ni–Fe–PGE–Au–Te–S systems (Figs. 11, 12). Finally, the high-temperature interval of the first stage (1100–800 °C) remains beyond the metasomatic paradigm for which there are numerous experimental data on the release of Pt and Pd bismuthotellurides and arsenides from sulfide liquids (Helmy et al., 2007, 2010; Sinyakova et al., 2017, 2019).

Particular attention is paid to the experimental evidence for possible splitting of PGE-Bi-Te-containing sulfide liquids at 920–825 °C with the formation of globules of immiscible, substantially telluride phases enriched in Bi and platinum metals (Helmy et al., 2007). These data argue for the existence of an immiscibility region of residual sulfide systems when critical values of Te/S are reached in a temperature range slightly higher than sulfide solidus accompanied by partial extraction of PGE into immiscible bismuthotelluride liquids. Figure 13 shows an oval heterogeneous assembly (possibly of section of a droplet-shaped inclusion), which is found in the specimen of the pegmatoid troctolite 13DV551-4a at the boundary between pyrrhotite and cubanite. The bright phase is froodite (Pd, Pt, Ir, Au)Bi_2, and the light gray one is Ru–Pt–Se–Pb-containing tellurium, where the Te content is slightly higher than 85 wt.%, and the total lead, selenium, and PGE is about 3 wt.% (the remaining elements are Fe, Cu, Cd, and O). The small sum for this analysis (92.5%) and the presence of oxygen does not allow one to consider these data as a reliable characterization of this phase, but this unusual finding is worth noting because it can be interpreted as evidence of segregation of immiscible PGE+Bi-containing telluride phase from sulfide liquid upon crystallization of mss ± iss solutions with subsequent phase exsolution (Helmy et al., 2007, 2010).

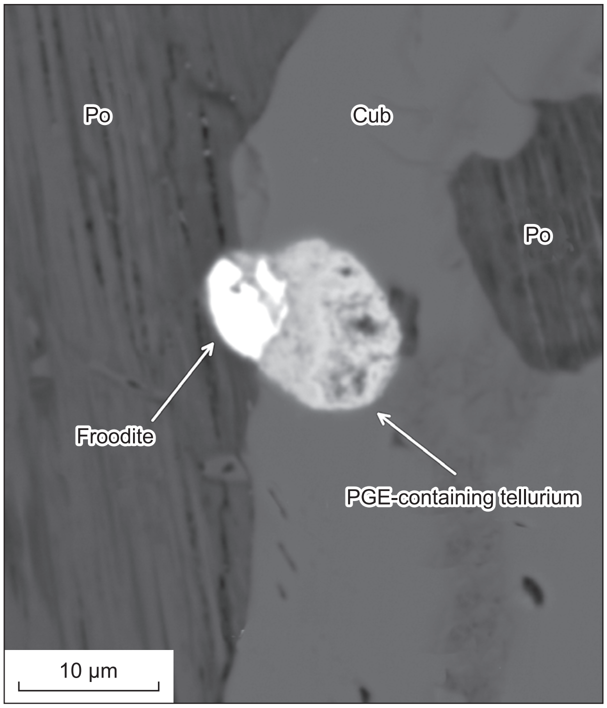

Fig. 13. Heterophase isolation of froodite and PGE-containing tellurium at the boundary between pyrrhotite and cubanite in the pegmatoid sulfide.

Further analysis of the possibility and experimental arguments in favor of the formation of PGMs in the field of subsolidus sulfide systems is beyond the scope of this article. It can be only noted that the long history of cooling the Dovyren cumulates (Ariskin et al., 2018b) suggests some annealing of original mineral assemblages and a collective recrystallization of primary grains of sulfides and related PGE minerals with the formation of more perfect crystals, possibly with participation of volatile components. It is very likely that the low-temperature stage of the second step is also accompanied by hydrothermal-metasomatic transformations of the newly formed phases under the influence of late magmatic fluids or superimposed (secondary) processes. This scenario almost leaves no chance for reconstructing the composition and conditions of the formation of the initial sulfide substance, provided that we rely only on the diagnostics of the observed mineral phases and the results of LA-ICP-MS studies of the sulfide compositions. This genetic record is present in the geochemistry of rocks, recalculated to 100% of the sulfide mass (Ariskin et al., 2018c).

CONCLUSIONS

The studies show that the carrier phase of noble metals, chalcogenes (Se and Te) and other chalcophile elements (Sn, Pb, Mo, and Cd) in troctolites is protosulfide melts and their derivatives. The geochemical features of these systems correspond to the crystallization products of the sulfide precursor, which is similar in composition to the immiscible sulfide liquid, established for the Dovyren basal ultramafics (Ariskin et al., 2018c). Thus, the question of the nature of a mobile agent that transports PGEs, gold, and silver in the strata of troctolite cumulates seems to be resolved from the physicochemical point of view. In this case, the problem of concentration of precious metals is transformed into the plane of specific physical mechanisms and characteristics of a heterogeneous medium (rheology, permeability, wetting by sulfide of different phases, etc.), in which the following is possible: a) spatial separation of iss-liquids from mss-restite, b) their infiltration downward, and c) mechanical accumulation at the boundaries of critically low permeability. It is noteworthy that the idea of isolating and accumulating low-temperature fractions of iss-like melts in intrusive bodies is not new (Mungall, 2007), but the material presented in this work for the first time demonstrates a comprehensive solution to the problem.

At this stage, it is difficult to determine the extent to which these observations and results are applicable to the anorthosites of the Main Reef with PGE-rich mineralization. According to a number of signatures, the geochemical characteristics of these rocks, the mineralogy of sulfides and PGMs are close to sulfide-bearing troctolites (Ariskin et al., 2018b; Orsoev, 2019; Spiridonov et al., 2019a,b). At the same time, subtle differences in the chemistry of the noble metal phases have been established (Spiridonov et al., 2019a), which should be taken into account when developing a generalized model for the differentiation and percolation of sulfides as a factor of concentration of noble metals in the Dovyren chamber.

Finally, regarding the hypothesis of fluid transfer of the PGE-rich material. It is widely believed among followers of these ideas that, as a transporting agent, the fluid flow is capable of "discharging" ore components and migrating further upward without actually leaving any geochemical traces in the mineralization zone. Such mechanisms can neither be proved nor disproved. But if this point of view is accepted, one has to admit that, in the case of the Dovyren troctolites, there are at least two types of such flows that carry S, Se, Te, Au, Ag, Cu, and PGEs in ratios corresponding to the crystallization laws of mss- and iss -sulfide solutions without mixing with each other and without interacting with flowing cumulates.

The authors are grateful to D. Hutchinson (CODES, Hobart, Australia) and E.M. Spiridonov (Moscow State University) for their help in identifying PGMs and the phase diversity of sulfides. We also greatly appreciate the help of Karsten Goemann and Sarah Gilbert from the University of Tasmania (Hobart, Australia) in making high-resolution video recordings and processing the results of LA-ICP-MS analyses. We express our gratitude to the scientific reviewers of this work — A.V. Sobolev, N.D. Tolstykh, and A.E. Izokh for their informative comments that improved the final version of the manuscript. This article is numbered 1384 at the ARC Centre of Excellence for Core to Crust Fluid Systems, Perth, Australia (http://www.ccfs.mq.edu.au).

This work was financially supported by the Russian Science Foundation (Grant No. 16-17-10129). Analytical studies in the Laboratory of local methods of material studies of the Department of Petrology of the Geological Faculty of Moscow State University are carried out using the JEOL JXA-8230 microanalyzer acquired at the expense of the Moscow University Development Program (analysts N.N. Korotaeva and V.O. Yapaskurt).

REFERENCES

Ariskin, A.A., Kostitsyn, Yu.A., Konnikov, E.G., Danyushevsky, L.V., Meffre, S., Nikolaev, G.S., McNeill A., Kislov, E.V., Orsoev, D.A., 2013. Geochronology of the Dovyren intrusive complex, northwestern Baikal area, Russia, in the Neoproterozoic. Geochem. Int. 51, 859–875.

Ariskin, A.A., Danyushevsky, L.V., Konnikov, E.G., Maas, R., Kostitsyn, Yu.A., McNeill, A., Meffre, S., G.S. Nikolaev, Kislov, E.V., 2015a. The Dovyren intrusive complex (northern Baikal region, Russia): isotope–geochemical markers of contamination of parental magmas and extreme enrichment of the source. Russian Geology and Geophysics (Geologiya i Geofizika) 56 (3), 411–434 (528–556).

Ariskin, A.A., Nikolaev, G.S., Danyushevsky, L.V., Kislov, E.V., Malyshev, A., Barmina, G.S., 2015b. New type of low-sulfide PGE mineralization in primitive troctolites from the Yoko-Dovyren layered massif, in: Proceedings of XII All-Russian Petrographic Conference [in Russian]. Petrozavodsk, Vol. 1, pp. 289–291.

Ariskin, A.A., Kislov, E.V., Danyushevsky, L.V., Nikolaev, G.S., Fiorentini, M.L., Gilbert, S., Goemann, K., Malyshev, A., 2016. Cu–Ni–PGE fertility of the Yoko-Dovyren layered massif (northern Transbaikalia, Russia): thermodynamic modeling of sulfide compositions in low mineralized dunite based on quantitative sulfide mineralogy. Mineral. Deposita 51, 993–1011.

Ariskin, A.A., Bychkov, K.A., Nikolaev, G.S., 2017a. Modeling of trace-element composition of sulfide liquid in a crystallizing basalt magma: Development of the *R*-factor concept. Geochem. Int. 55 (5), 465–473.

Ariskin, A.A., Fomin, I.S., Zharkova, E.V., Kadik, A.A., Nikolaev, G.S., 2017b. Redox conditions during crystallization of ultramafic and gabbroic rocks of the Yoko-Dovyren massif (Based on the results of measurements of intrinsic oxygen fugacity of olivine). Geochem. Int. 55 (7), 595–607.

Ariskin, A.A., Bychkov, K.A., Nikolaev, G.S., Barmina, G.S., 2018a. The COMAGMAT-5: Modeling the effect of Fe–Ni sulfide immiscibility in crystallizing magmas and cumulates. J. Petrol. 59, 283–298.

Ariskin, A., Danyushevsky, L., Nikolaev, G., Kislov, E., Fiorentini, M., McNeill, A., Kostitsyn, Yu., Goemann, K., Feig, S., Malyshev, A., 2018b. The Dovyren Intrusive Complex (Southern Siberia, Russia): Insights into dynamics of an open magma chamber with implications for parental magma origin, composition, and Cu-Ni-PGE fertility. Lithos 302–303, 242–262.

Ariskin, A.A, Nikolaev, G.S., Danyushevsky, L.V., Fiorentini, M., Kislov, E.V., Pshenitsyn, I.V., 2018c. Genetic interpretation of the distribution of PGE and chalcogens in sulfide-mineralized ultramafic rocks from the Yoko-Dovyren layered intrusion. Geochem. Intern. 56, 1322–1340.

Barkov, A.Yu., Nikiforov, A.A., 2015. A new criterion in prospecting for zones of pge-bearing mineralization of the "Kivakka reef"-type. Vestnik Voronezhskogo gosudarstvennogo universiteta. Seriya Geologiya, No. 4, 75–83.

Barnes, S.-J., Prichard, H.M., Cox, R.A., Fisher, P.C., Godel, B., 2008. The location of the chalcophile and siderophile elements in platinum-group element ore deposits (a textural, microbeam and whole rock geochemical study): Implications for the formation of the deposits. Chem. Geol. 248, 295–317.

Boudreau, A.E., McCallum, I.S, 1992a. Infiltration metasomatism in layered intrusions – An example from the Stillwater Complex, Montana. J. Volcanol. Geotherm. Res. 52, 171–183.

Boudreau, A.E., McCallum, I.S., 1992b. Concentration of platinum-group elements by magmatic fluids in layered intrusions. Econ. Geol. 87, 1830–1848.

Brenan, J.M., 2015. Se–Te fractionation by sulfide–silicate melt partitioning: Implications for the composition of mantle-derived magmas and their melting residues. Earth Planet. Sci. Lett. 422, 45–57.

Cabri, L.J., 1973. New data on phase relations in the Cu-Fe-S system. Econ. Geol. 68, 443–454.

Campbell, I.H., Naldrett, A.J., 1979. The influence of silicate: sulfide ratios on the geochemistry of magmatic sulfides. Econ. Geol. 74, 1503–1506.

Cawthorn, R.G., 1994. Formation of chlor- and fluor-apatite in layered intrusions. Mineral. Mag. 58, 299–306.

Chung, H.-Y., Mungall, J.E., 2009. Physical constraints on the migration of immiscible fluids through partially molten silicates, with special reference to magmatic sulfide ores. Earth Planet. Sci. Lett. 286, 14–22.

Craig, J.R., 1971. Violarite stability relations. Am. Mineral. 56, 1303–1311.

Craig, J.R., 1973. Pyrite-pentlandite assemblages and other low-temperature relations in the Fe–Ni–S systems. Am. J. Sci. 273A, 496–510.

Craig, J.R., Kullerud, G., 1968. The Cu–Fe–Ni–S system. Carnegie Inst. Washington, Yearbook, Vol. 66, 413–417.

Distler, V.V., Sinyakova, E.F., Kosyakov, V.I., 2016. Behavior of noble metals upon fractional crystallization of copper-rich sulfide melts. Dokl. Earth Sci. 469 (2), 811–814.

Distler, V.V., Stepin, A.G., 1993. Low-Sulfide PGE-bearing unit of the Yoko-Dovyren layered ultrabasic-basic intrusion (Northern Baikal region). Dokl. Akad. Nauk 328, 498–501.

Ernst, R.E., Hamilton, M.A., Söderlund, U., Hanes, J.A., Gladkochub, D.P., Okrugin, A.V., Kolotilina, T., Mekhonoshin, A.S., Bleeker, W., LeCheminant, A.N., Buchan, K.L., Chamberlain, K.R., Didenko, A.N., 2016. Long-lived connection between southern Siberia and northern Laurentia in the Proterozoic. Nat. Geosci. 9, 464–469.

Godel, B., 2015. Platinum-group element deposits in layered intrusions: recent advances in the understanding of the ore forming processes, in: Charlier, B., Namur, O., Latypov, R., Tegner, C. (Eds.), Layered Intrusions. Springer, Dordrecht, pp. 379–432.

Godel, B., Barnes, S.-J., Maier, W.D., 2007. Platinum-group elements in sulphide minerals, platinum-group minerals, and whole-rocks of the Merensky Reef (Bushveld Complex, South Africa): Implications for the formation of the reef. J. Petrol. 48, 1569–1604.

Gurulev, S.A., 1965. Geology and Genesis of the Yoko-Dovyren Gabbro-Peridotite Pluton [in Russian]. Nauka, Moscow.

Helmy, H.M., Ballhaus, C., Berndt, J., Bockrath, C., Wohlgemuth-Ueberwasser, C., 2007. Formation of Pt, Pd and Ni tellurides: experiments in sulfide–telluride systems. Contrib. Mineral. Petrol. 153, 577–591.

Helmy, H.M., Ballhaus, C., Wohlgemuth-Ueberwasser, C., Fonseca, R.O.C., Laurenz, V., 2010. Partitioning of Se, As, Sb, and Bi between monosulfide solid solution and sulfide melt – application to magmatic sulfide deposits. Geochim. Cosmochim. Acta 74, 6174–6179.

Holness, M.B., Vukmanovic, Z., Mariani, E., 2017. Assessing the role of compaction in the formation of adcumulates: a microstructural perspective. J. Petrol. 58, 643–673.

Holwell, D.A., Keays, R.R., McDonald, I., Williams, M.R. 2015. Extreme enrichment of Se, Te, PGE and Au in Cu sulfide microdroplets: evidence from LA-ICP-MS analysis of sulfides in the Skaergaard Intrusion, east Greenland. Contrib. Mineral. Petrol. 170, Article 53.

Holwell, D.A., McDonald, I., 2007. Distribution of platinum group elements in the Platreef at Overysel, northern Bushveld Complex: a combined PGM and LA ICP–MS study. Contrib. Mineral. Petrol. 154, 171–190.

Jarosewich, E., Nelen, J.A., Norberg, J.A., 1980. Reference samples for electron microprobe analysis. Geostand. Newslett. 4, 43–47.

Kislov, E.V., 1998. The Yoko-Dovyren Layered Pluton [in Russian]. BNTs SO RAN, Ulan-Ude.

Konnikov, E.G., 1986. Differentiated Ultrabasic-Basic Complexes in the Precambrian Rocks of Transbaikalia [in Russian]. Nauka, Novosibirsk.

Konnikov, E.G., Meurer, W.P., Neruchev, S.S., Prasolov, E.M., Kislov, E.V., Orsoev, D.A., 2000. Fluid regime of platinum group elements (PGE) and gold-bearing reef formation in the Dovyren mafic-ultramafic layered complex, eastern Siberia, Russia. Mineral. Deposita 35, 526–532.

Kullerud, G., Yund, R.A., Moh, G.H., 1969. Phase relations in the Cu–Fe–S, Cu–Ni–S and Fe–Ni–S systems. Econ. Geol. Monograph 4, 323–343.

Maier, W.D., 2005. Platinum-group element (PGE) deposits and occurrences: Mineralization styles, genetic concepts, and exploration criteria. J. African Earth Sci. 41, 165–191.

Manuilova, M.M., Zarubin, V.V., 1981. Precambrian Volcanogenic Rocks of the Northern Baikal Region [in Russian]. Nauka, Leningrad.

Mungall, J.E., 2005. Magmatic geochemistry of the platinum-group elements. Exploration for platinum-group elements deposits. Short Course Ser. (Mineral Assoc Canada) 35, 1–34.

Mungall, J.E., 2007. Crystallization of magmatic sulfides: An empirical model and application to Sudbury ores. Geochim. Cosmochim. Acta 71, 2809–2819.

Mungall, J.E., Brenan, J.M., 2014. Partitioning of platinum-group elements and Au between sulfide liquid and basalt and the origins of mantle-crust fractionation of the chalcophile elements. Geochim. Cosmochim. Acta 125, 265–289.

Naldrett, A.J., 2004. Magmatic Sulfide Deposits: Geology, Geochemistry and Exploration. Springer-Verlag, Heidelberg, Berlin.

Oberthür, T., 2011. Platinum-group element mineralization of the Main Sulfide Zone, Great Dyke, Zimbabwe. Rev. Econ. Geol. 17, 329–349.

O'Driscoll, B., González-Jiménez, J.M., 2016. Petrogenesis of the platinum-group minerals. Rev. Mineral. Geochem. 81, 489–578.

Orsoev, D.A., 2019. Anorthosites of the low-sulfide platiniferous horizon (Reef I) in the upper Riphean Yoko-Dovyren massif (Northern Cisbaikalia): New data on the composition, PGE–Cu–Ni mineralization, fluid regime, and formation conditions. Geol. Ore Depos. 61 (4), 306–332.

Orsoev, D.A., Kislov, E.V., Konnikov, E.G., Kanakin, S.V., Kulikova, A.B., 1995. Localization appropriateness and composition specific features of platinum-bearing horizons of the Ioko-Dovyren layered massif (Northern Transbaikalia). Dokl. Akad. Nauk 340, 225–228.

Orsoev, D.A., Mekhonoshin A.S., Kanakin S.V., Badmatsyrenova R.A., Khromova E.A., 2018. Gabbro-peridotite sills of the Late Riphean Dovyren plutonic complex (northern Baikal area, Russia) Russian Geology and Geophysics (Geologiya i Geofizika) 59 (5), 472–485 (589–605).

Queffurus, M., Barnes, S.-J., 2015. A review of sulfur to selenium ratio in magmatic nickel–copper and platinum-group element deposits. Ore Geol. Rev. 69, 301–324.

Raghavan, V., 2004. Cu–Fe–S (Copper–Iron–Sulfur). J. Phase Equil. Diffus. 25 (5), 450–454.

Rytsk, E.Yu., Shalaev, V.S., Rizvanova, N.G., Krymskii, R.Sh., Makeev, A.F., Rile, G.V., 2002. The Olokit Zone of the Baikal Fold Region: new isotopic geochronological and petrochemical data. Geotectonics 36, 24–35.

Sinyakova, E., Kosyakov, V., Palyanova, G., Karmanov, N., 2019. Experimental modeling of noble and chalcophile elements fractionation during solidification of Cu–Fe–Ni–S melt. Minerals 9, Article 531.

Sinyakova, E.F., Kosyakov, V.I., Borisenko, A.S., 2017. Effect of the presence of As, Bi, and Te on the behavior of Pt metals during fractionation crystallization of sulfide magma. Dokl. Earth Sci. 477, 1422–1425.

Sinyakova, E.F., Kosyakov, V.I., Borisenko, A.S., Karmanov, N.S., 2019. Behavior of noble metals during fractional crystallization of Cu–Fe–Ni–(Pt, Pd, Rh, Ir, Ru, Ag, Au, Te) sulfide melts. Russian Geology and Geophysics (Geologiya i Geofizika), 60 (6), 642–661 (820–842).

Sinyova, S.I., Kosyakov, V., Sinyakova, E.F., Novoghilova, O.S., 2018. Crystallization of the quasibinary bnss-tss eutectic in the Cu–Fe–Ni–S system. Kondensirovannye sredy i mezhfaznye granitsy 20 (4), 650–658.

Smith, J.W., Holwell, D.A., McDonald, I., Boyce, A.J., 2016. The application of S isotopes and S/Se ratios in determining ore-forming processes of magmatic Ni–Cu–PGE sulfide deposits: A cautionary case study from the northern Bushveld Complex. Ore Geol. Rev. 73, 148–174.

Spiridonov, E.M., 2010. Ore-magmatic systems of the Noril'sk ore field. Russian Geology and Geophysics (Geologiya i Geofizika) 51 (9), 1059–1077 (1356–1378).

Spiridonov, E.M., Orsoev, D.A., Ariskin, A.A., Kislov, E V., Korotaeva, N.N., Nikolaev, G.S., Yapaskurt, V.O., 2019. Germanium-rich palladium minerals palladogermanide Pd_2Ge, paolovite $Pd_2(Sn, Ge)$, and zvyagintsevite in sulfide-bearing anorthosites of the Yoko-Dovyren Pluton, Baikal Area. Geochem. Int. 57 (5), 600–603.

Spiridonov, E.M., Orsoev, D.A., Ariskin, A.A., Korotaeve, N.N., Yapaskurt, V.O., Orsoev, D.A., Kislov, E.V., Nikolaev, G.S., 2019. Hg- and Cd-bearing Pd, Pt, Au, and Ag minerals in sulfide-bearing mafic and ultramafic rocks of the Yoko-Dovyren intrusion in the Baikalides of the northern Baikal area. Geochem. Int. 57 (1), 42–55.

Tolstykh, N.D., Orsoev, D.A., Krivenko, A.P., Izokh, A.E., 2008. Noble-Metal Mineralization in Layered Ultrabasic–Basic Massifs of the Southern Siberian Platform [in Russian]. Parallel', Novosibirsk.

Tsujimura, T., Kitakaze, A., 2004. New phase relations in the Cu–Fe–S system at 800 °C; constraint of fractional crystallization of a sulfide liquid. Neues Jahrb. Mineral. Monatsh., 10, 433–444.